JPL PUBLICATION 79-34

Diagnosis of Cutaneous Thermal Burn Injuries by Multispectral Imaging Analysis

Victor J. Anselmo
Bruce E. Zawacki

September 1, 1978

National Aeronautics and Space Administration

Jet Propulsion Laboratory
California Institute of Technology
Pasadena, California

JPL PUBLICATION 79-34

Diagnosis of Cutaneous Thermal Burn Injuries by Multispectral Imaging Analysis

Victor J. Anselmo
Jet Propulsion Laboratory

Bruce E. Zawacki
Los Angeles County/University of Southern California
Medical Center

September 1, 1978

National Aeronautics and
Space Administration

Jet Propulsion Laboratory
California Institute of Technology
Pasadena, California

The research described in this publication was carried out by the Jet Propulsion Laboratory, California Institute of Technology, under NASA Contract No. NAS7-100.

ABSTRACT

This document is the final report on the burns diagnosis studies conducted by the Jet Propulsion Laboratory for the National Aeronautics and Space Administration. The studies utilized image processing technology developed for use in planetary, lunar, and earth surface analysis. The work was conducted with the cooperation of the Los Angeles County/University of Southern California Medical Center and was performed at that facility.

Special photographic or television image analysis is shown to be a potentially useful technique to assist the physician in the early diagnosis of thermal burn injury. This report presents a background on the medical and physiological problems of burns and discusses the proposed methodology for burns diagnosis from both the theoretical and clinical points of view. The television/computer system constructed to accomplish this analysis is described, and the clinical results are discussed.

CONTENTS

Figures

Tables

SECTION I

INTRODUCTION

A. BACKGROUND

This report summarizes a study made to determine a method of diagnosing burn injury. The study was conducted under the sponsorship and funding of the National Aeronautics and Space Administration with co-funding from the Los Angeles County-University of Southern Medical Center in Los Angeles, California and from the AGA Corporation in Secaucus, New Jersey. The report presents a background on the medical and physiological problem of burns and discusses the methods of diagnosis used from both the theoretical and clinical points of view, presents a description of a stand-alone system designed and built at the Jet Propulsion Laboratory to accomplish this diagnostic work, and presents the initial clinical data obtained from this system.

Burn injuries are an increasingly serious medical problem in the United States. During 1971, for example, approximately 2 million people incurred burn injuries, almost double the number reported for 1967. Of the 300,000 who suffered burns severe enough to cause disability, 30,000 required prolonged intensive care for an average hospital stay of 64 days. Despite excellent intensive care, 38% of the hospitalized patients died from undefined biochemical and physiological changes or from infections (NIH, 1973). There is no reason to suppose that the problem has become less severe.

The classification of burn injuries remains an area of considerable confusion. The popular description of first, second, and third degrees was defined over 150 years ago. This classification is based on the superficial appearance of the injury and was used with minor modifications until about 30 years ago, when burn physicians began to realize that it was the depth of injury that was of prime importance and not the superficial appearance. Thus there evolved a two-category description which is defined as follows: The partial-thickness burn is a wound in which sufficient epithelial elements remain to allow spontaneous skin repair, and the full-thickness burn is a wound in which the elements necessary for spontaneous skin repair have been destroyed. In the latter case, skin repair can occur by contraction of the wound and cell migration from the edge if the area of injury is only a few square centimeters or less. When this peripheral regrowth is not possible or sufficient, grafting is necessary.

The range of injuries covered by these two categories is extensive, and in a clinical situation the two cannot always be distinguished from each other. The more central areas of the range, i.e., the very deep partial-thickness or the more shallow full-thickness injuries are very difficult or impossible to diagnose, often until 4 to 6 weeks after the injury when the course of healing becomes obvious. It is the early diagnosis of this region or category of burns which has been the object of the work presented herein.

Necrotic tissue covers the full-thickness burn. This tissue either sloughs off with time or is removed surgically. In many cases, surgical debridement can be accomplished within a few days postburn if an accurate diagnosis of burn depth can be made. This early removal of necrotic skin is called early tangential excision and is gaining popularity among burn physicians.

The success of early tangential excision and grafting of the full-thickness burn is impressive, and it is now generally accepted that this treatment is advantageous for thermal burns of less than 15 to 25% of total body surface area (Jackson, 1969; Janzekovic, 1970; Monafo, et al., 1972). A continuing problem with the optimal application of this technique in many cases is the inability of the physician to produce an early and accurate diagnosis of the depth of the skin loss. Hinshaw (1961) states, "No one questions the importance of distinguishing between second and third degree burns, and everyone knows the task is difficult and sometimes impossible." Jackson (1961) noted "The ability to make this diagnosis on the day of burning is of very great practical value in deciding whether to excise a burn or not." Early removal of the irreversibly destroyed tissue has many advantages. It reduces the risk of infection, the occurrence of fibrosis, and the loss of function to the damaged limb. It also appears to provide the best surgical results in the shortest time (Jackson and Stone, 1972). However, in many cases, it is impossible to differentiate between areas of full-thickness injury and areas which would spontaneously heal with time. Treatment of these questionable areas then depends quite heavily on the intuition and experience of the physician. Even though he is aided by many tools covering sensory, mechanical, and thermal phenomena, the only positive method available to him is to wait for 4 to 6 weeks until the natural healing pattern is established and areas of irreversibly damaged and necrotic tissue are indicated. If the physician decides to excise tissue before a precise diagnosis is avaiable, the patient may suffer by not having sufficient tissue removed. Residual necrotic tissue would then remain as a source of sepsis and would ultimately require additional surgery, pain, and expense. In the case of large burns, if excessive tissue were excised, the patient would suffer from the unnecessary removal of skin able to heal spontaneously. This error might also increase the risk of sepsis by enlarging the wound area or reducing the supply of skin available for use as graft. In any case, a delay or inaccuracy in the diagnosis of the irreversibly damaged tissue increases the danger of sepsis, which is a primary cause of death for the burned patient.

The logic behind seeking a quantitative basis for a more precise diagnosis is compelling, and a search was made for a method that would identify and differentiate varying depths of dermal necrosis. The method used in this work is called multispectral imaging analysis and is derived from technology developed by NASA for planetary, lunar, and earth studies (Goetz, et al., 1975).

The rationale for the multispectral photographic approach to this problem derives from the understanding of the early appearance of the burn (Jackson, 1953) and the most sensitive diagnostic method available to date, i.e., the visual observation of the burn surface (the skin reflectance patterns) by the physician. Indeed, this is the primary basis for the categorization of first, second, and third degree injury. For example, in white light the hyperaemic zone at the periphery of a burn appears red because all other wavelengths (colors) other than red are absorbed by the tissue. Red light remains to be reflected and "seen" by the observer. A parchment-appearing zone of stasis appears because no wavelengths are absorbed to the extent that the reflected light significantly changes color. In this case the observer sees the original light reflected back with little change.

B. BURN WOUND PHYSIOLOGY

Figure 1 shows a model of a cross section of human skin, indicating partial-thickness burn by the depth of shading. The outer layer of the skin is the epidermis, the middle layer is the dermis, and the lower layer is the fatty tissue. Of particular interest is the presence and depth of the hair follicles and the sweat glands. The base of these structures is surrounded with cells capable of forming new "skin." These cells lie very close to the interface of the dermis and the subcutaneous fat, and represent the vital plane insofar as spontaneous skin repair is concerned. If destruction occurs below this plane, the burn is full-thickness in depth; if above the plane, destruction is partial-thickness.

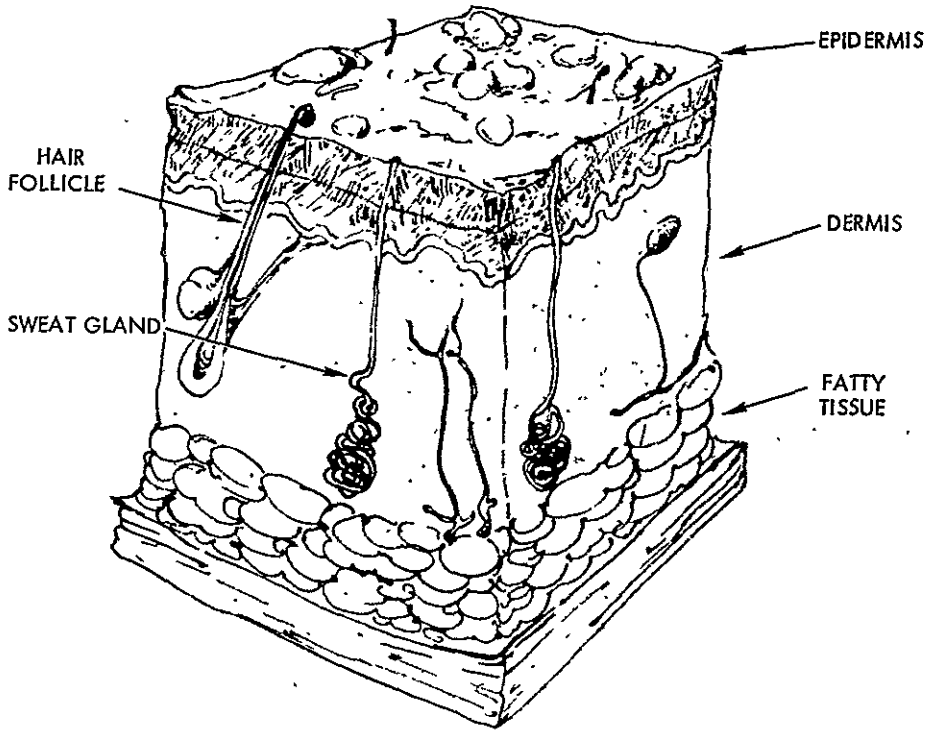

Figure 1. Partial-Thickness Burn

In the area of the junction of the dermis with the subcutaneous fat there exists a plane of large, macroscopically visible arterioles and venules which are roughly parallel to the skin surface. Branched from this plane are a series of smaller arterioles and venules which are perpendicular to the plane of the skin and are continuous with the capillaries in the dermis. This structure is important from a diagnostic point of view since if the deep venous structure in this area can be shown to be coagulated, full-thickness burn is present (Jackson, 1969).

Figure 2 shows a full-thickness wound. Note that destruction of the tissue, as indicated by shading, has occurred through the deep dermal layer and into the fatty tissue. No cells remain viable for the formation of new skin. The differentiation between full- and partial-thickness burn is shown explicitly in Figures 3 and 4. These are cleared tissue sections from a rat subjected to laboratory burns and followed after 24 hours with an intra-arterial injection of India ink. Figure 3 shows the partial-thickness wound. Note that the venous structure at the base of the dermis is intact and the bulbous bases of hair follicles are surrounded by intact capillaries. Because the dermal base and the base of hair follicles remain vascularized and viable, the wound is partial-thickness in depth (Zawacki and Jones, 1967).

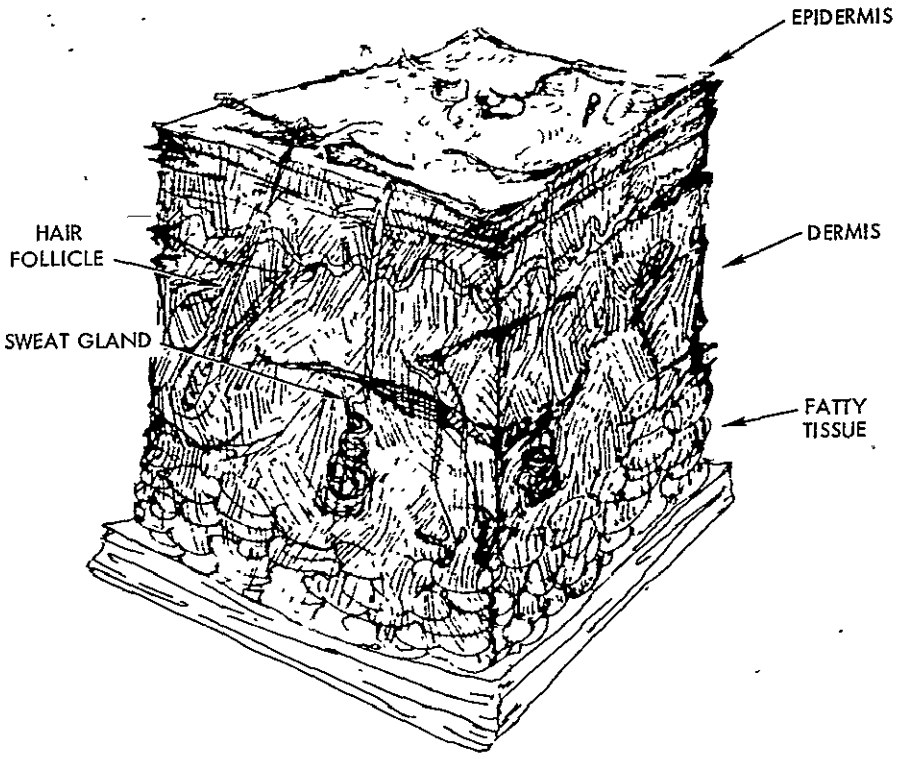

Figure 2. Full-Thickness Burn, Showing Injury to All Layers

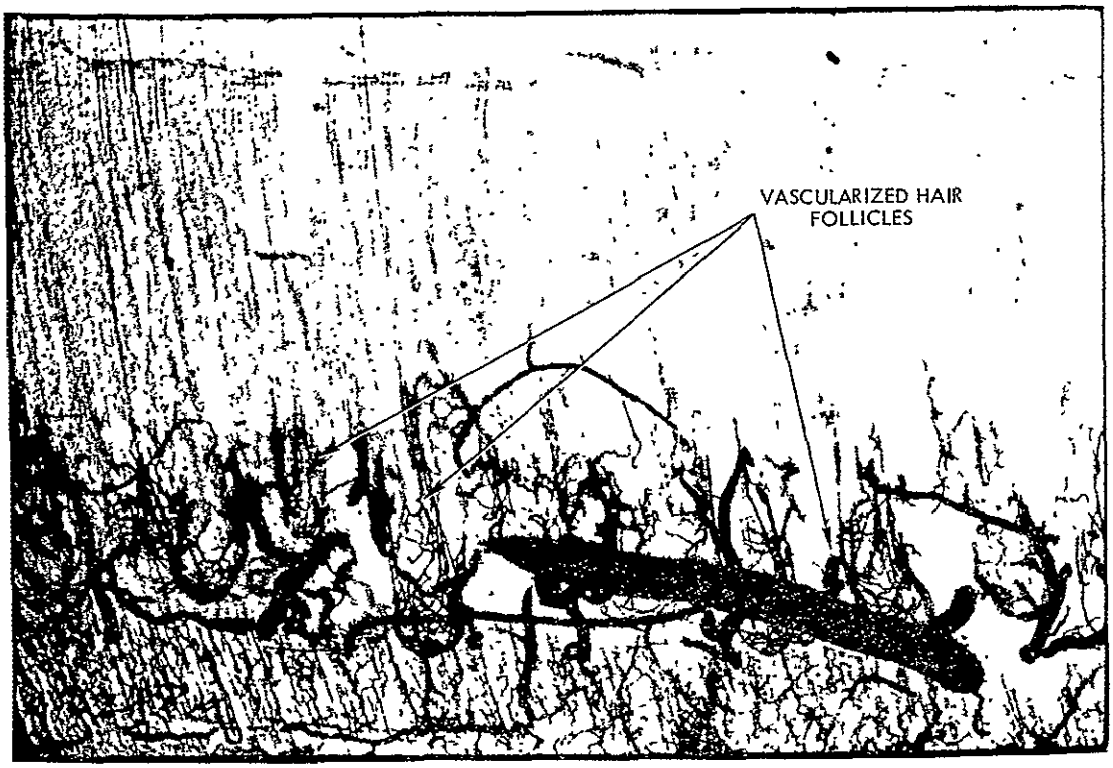

Figure 3. Partial-Thickness Wound in Rat Skin Subjected to a Laboratory Burn

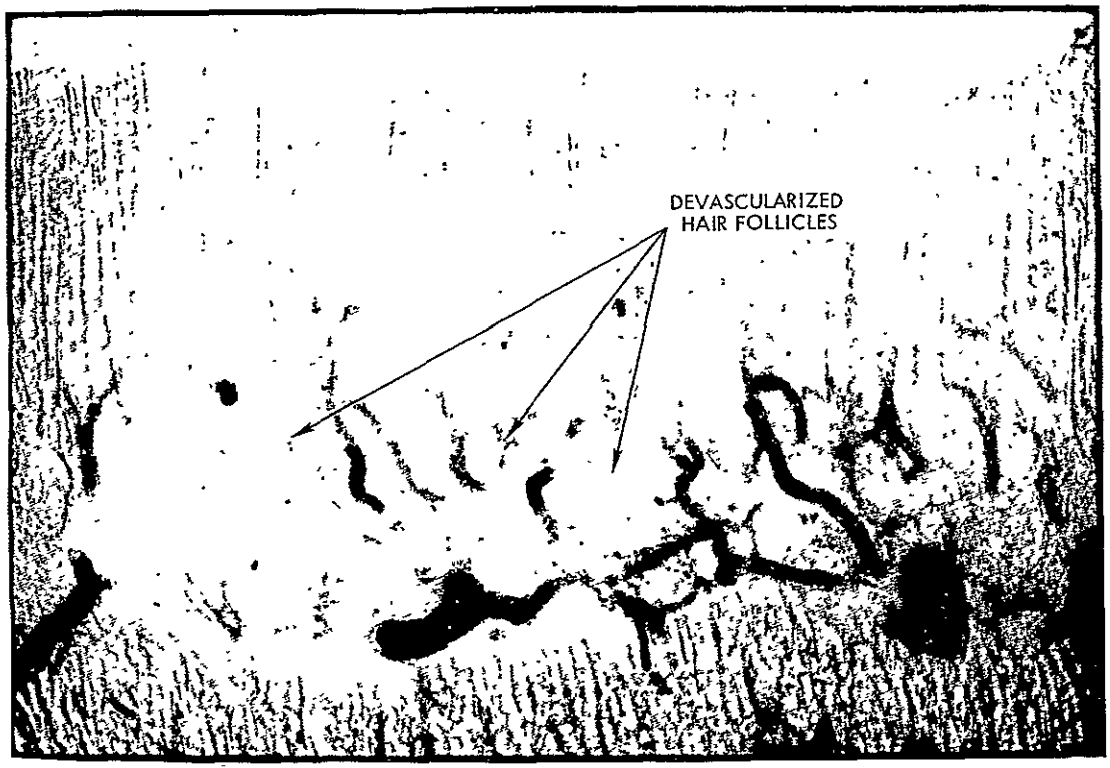

Figure 4. Full-Thickness Wound in Rat Skin Subjected to a Laboratory Burn

Compare this now to Figure 4. Note the devascularization of the dermal base and hair follicles indicated by the broken and coagulated vascular structure. This results in a full-thickness burn and suggests that a diagnostic approach utilizing a method which could detect this devascularization over large areas of skin could be effective. The dynamic appearance of the burn wound may be summarized as follows: During the first week after the injury, the wound is characterized by three zones: the zone of hyperaemia, the zone of stasis, and the zone of coagulation. The zone of hyperaemia presents the most superficial wound. This zone appears red and continues to exhibit adequate circulation and metabolism necessary for viability. By the seventh day the wound is dry and healed with complete regeneration of the epidermis but no apparent damage to the dermis. This results in a partial-thickness injury.

The zone of stasis initially appears very much like the zone of hyperaemia, but upon testing, one finds that metabolic processes are absent. At the end of 24 hours, circulation ceases and complete stasis of the affected vascular system occurs. Between the third and seventh days, the zone of stasis turns brownish-white because the superficial surface of the dermis is avascular and necrotic, and the red cells which had previously colored the zone have been hemolyzed and the contents thermally denatured. This zone may be partial- or full-thickness injury.

The zone of coagulation appears brownish-white and is characterized by complete obliteration of the lumina of the vessels in the subpapillary plexus and the coagulation of the tissue. The zone may result in deep partial- or full-thickness injury.

It may be desirable to excise the full-thickness burn early, during the first week if possible. Although it is known that the tissue of the zones of coagulation and stasis will be lost, it is not possible by inspection to determine whether these zones include the full thickness of the skin or not. If excision is performed before a precise diagnosis of the full-thickness burn area is made, the patient may suffer because sufficient tissue was not removed. Residual necrotic tissue will then remain as a source of sepsis requiring additional debridement, accompanied by additional pain and expense. If an excess of tissue is removed, the patient may suffer due to loss of viable tissue necessary for the healing process.

C. RATIONALE

In seeking a method for the early determination of deep coagulation and therefore of full-thickness burn, infrared photography* was considered as a potential method to indicate the devascularization and thermal denaturation associated with the full-thickness burn. Deoxygenated blood has a moderate absorptance in the very near infrared.

*Infrared photography does not detect temperature patterns at temperatures associated with skin, even after burns, but indicates the absorption or reflection of light beyond the visible spectrum.

One may therefore reason that infrared patterns of thrombosed or coagulated venous structure, occurring in zones of stasis or coagulation, could be an indication of full-thickness burn. This is because the venous structure capable of detection by infrared photography occurs at dermal depths associated with the cellular elements necessary for spontaneous regrowth of the skin. Typical penetration of the infrared is 2-5 mm through the skin. This would coincide with the base of the hair follicles and the plexus of vessels which, if containing thermally denatured (and hemolyzed red cells) would be a direct indication of destruction of the basal cells surrounding the root of the hair follicle. These are the deepest elements available for the spontaneous healing of the skin, should total thermal destruction occur above these elements.

The colorimetry of the burn wound also held suggestions of other spectral areas of potential interest. The zone of hyperaemia, appearing bright red, suggested the use of a region within the red spectrum. The zone of stasis, tending to be a parchment-white, suggested the use of a color not normally appearing on healthy or thermally injured skin since a high spectral reflectance would occur in the zone of stasis. A filter in the green spectrum was chosen.

The analytical approach thus consisted of using infrared light, which penetrates deepest, to investigate the thermal denaturation of the superficial arterioles and venules for indications of a full-thickness injury; red light, which does not penetrate as deep as infrared, for characterizing zones of hyperaemia; and green light, which is the least penetrating, to differentiate the zones of stasis from those of coagulation and hyperaemia, as well as from normal skin.

SECTION II

PHOTOGRAPHIC ANALYSIS

A. THEORY

Let the image produced through a red filter be referred to as I_R, that produced through a green filter as I_G, and that produced through an infrared filter as I_{IR}.

A photographic image I is the response of the film to the incident light energy reflected from a target. For a black and white transparency, it is characterized as the spatial distribution of the optical density over the image. The exposure distribution $E_{\Delta\lambda}$, which causes this image, can be written as

$$E_{\Delta\lambda} = t_E Z^*(x',y') \int_{\Delta\lambda} i_o(x',y',T_0,\lambda)\rho(x',y',\lambda)\tau_s(\lambda)\tau_f(\lambda)S_f(\lambda)d\lambda \tag{1}$$

where

γ	=	film gamma
t_E	=	time of exposure
$Z^*(x',y')$	=	geometric factor relating the relative positions of the source, the target, and the camera
(x',y')	=	Cartesian coordinate position on the image
$i_o(x',y',T_0,\lambda)$	=	intensity function of the source
T_0	=	source temperature
λ	=	wavelength
$\rho(x',y',\lambda)$	=	reflectance function of the target
$\tau_s(\lambda)$	=	transmission function of the camera system
$\tau_f(\lambda)$	=	transmission bandpass of the filter system
$S_f(\lambda)$	=	sensitivity of the film
$\Delta\lambda$	=	net bandpass defined by film sensitivity and by the camera system and filter systems

The preceding equation can be simplified to

$$E_{\Delta\lambda} = t_E Z^*(x',y') \int_{\Delta\lambda} \rho(x',y',\lambda)\psi(x',y',\lambda)d\lambda \tag{2}$$

For multiple functions of a single integral, the mean value theorem allows

$$E_{\Delta\lambda} = t_E Z^*(x',y')\bar{\rho}_{\Delta\lambda} \int_{\Delta\lambda} \psi(x',y',\lambda)d\lambda \tag{3}$$

The optical density of the image $I_{\Delta\lambda}$ is related to the exposure by

$$I_{\Delta\lambda} = \gamma \log (E_{\Delta\lambda}) + \text{const} \tag{4}$$

or

$$I_{\Delta\lambda} = \gamma \log \left(t_E Z^*(x',y')\rho_{\Delta\lambda} \int_{\Delta\lambda} \psi(x',y',\lambda)d\lambda \right) + \text{const.} \tag{5}$$

Now let $I_{\Delta\lambda_i}$ be the optical density function as determined by the digitization of a photograph filtered in region $\Delta\lambda_i$, and let $I_{\Delta\lambda_j}$ be the function for a second photograph of the same target filtered in another spectral region $\Delta\lambda_j$. Subtracting the values of the optical densities yields

$$I_{\Delta\lambda_i} - I_{\Delta\lambda_j} = \log \left\{ \frac{\left[t_{E_i} Z^*_i(x',y')\bar{\rho}_{\Delta\lambda_i} \int_{\Delta\lambda_i} \psi(x',y',\lambda)d\lambda \right]^{\gamma_i}}{\left[t_{E_j} Z^*_j(x',y')\bar{\rho}_{\Delta\lambda_j} \int_{\Delta\lambda_j} \psi(x',y',\lambda)d\lambda \right]^{\gamma_j}} \right\} + \text{const.} \tag{6}$$

In general, for uniform illumination of the target, it can be said that

$$\left\{ t_{E_i} Z_i^*(x',y') \int_{\Delta\lambda_i} \psi(x',y',\lambda)\,d\lambda \right\}^{\gamma_i} =$$

$$\text{const.} \times \left\{ t_{E_j} Z^*_j(x',y') \int_{\Delta\lambda_j} \psi(x',y',\lambda)\,d\lambda \right\}^{\gamma_j} \qquad (7)$$

so that

$$I_{\Delta\lambda_i} - I_{\Delta\lambda_j} = \log \left\{ \frac{(\bar{\rho}_{\Delta\lambda_i})^{\gamma_i}}{(\bar{\rho}_{\Delta\lambda_j})^{\gamma_j}} \right\} + \text{const.} \qquad (8)$$

Equation (8) states that the difference in the optical densities of the images filtered in the wavelengths regions $\Delta\lambda_i$ and $\Delta\lambda_j$ becomes a function of only the ratio of the mean value of the reflectances within the appropriate spectral regions. This ratio is dependent on the nature of the reflecting surface and may be characteristic or diagnostic of perturbations of that surface from some normal condition.

This is the basic methodology which has been derived for the burn analysis. The multispectral data are taken from three images of the burn wound, each image in one of the spectral regions. From the images, three functions are derived which depend on the ratio of the spectral reflectances of the skin, thereby allowing an analysis of a character of the burn which depends on a physical characteristic of the injured tissue - its reflectance.

B. EXPERIMENTAL METHOD

The original work of this task in burn wound diagnosis by imaging was based on an infrared photographic approach (Anselmo and Zawacki, 1973). This technique worked well for the identification of the full-thickness injury but did not allow the differentiation of other classifications of thermal injury. To accomplish this differentiation the multispectral approach was taken (Anselmo and Zawacki, June 1977). This method utilized three film cameras to obtain simultaneous filtered photographic images on 35 mm panchromatic films. Xenon flash lamps were used to illuminate the subject, and reflectance data within the spectral bands at 550, 620, and 800 nm were obtained. After standard processing

of the film, the 35 mm transparencies were scanned and digitized by an optical scanner using 25 μm pixel areas. The three spectral images were registered using a computer program which provided the proper geometric distortion for two of the three images so that sufficient overlap of the burn area of the images would result. Contrast enhancement by a linear stretch of the images assured complete use of the 256 level dynamic range of gray scale available from the image digitizer.

The difference between each pair of the three images was taken and used to produce three new images, each of which is proportional to the ratio of the reflectance of the target in the appropriate spectral regions. This is shown by Eqn. (8). These resulting digital images were contrast-enhanced to assure optimization of dynamic range capabilities. Each image was used to produce a photographic transparency with a device which exposes film by a flying spot beam whose intensity is controlled in proportion to the data number of the digital image. These transparencies were developed in a standard fashion and were mechanically registered so that when each was used with an assigned red, green, or blue lamp to expose photographic color print paper, there resulted a pseudocolor image. The color distribution on the image is determined by the ratio of the target reflectances and therefore was characteristic of the depth of the burn injury. This process will be discussed in more detail in Section IV of the report.

In the experimental procedure, three 35 mm cameras were used to take simultaneous photographs of the burn injury. Two of the cameras contained Kodak Plus X (black and white) film. One of these cameras used a Wratten 25A (red) filter and the other an X1 (yellow-green) filter. The third camera contained Kodak High Speed Infrared film (black and white) and used a Wratten 89A (infrared) filter. Both filters and film were standard, commercially available items.

The apparatus and spectral regions were chosen after numerous investigations using various combinations of readily available photographic filters to obtain maximum differentiation between partial- and full-thickness injuries. Honeywell Auto Strobonar 882 flash lamps were used as the light source. The photographs were taken in a darkened room so that the only illumination was from the strobe lamps. This method eliminated synchronization requirements for the camera shutters. The shutters were opened in unison by a pneumatic device, the flash was produced, and the shutters were closed. Three simultaneous images of the injured area were thus produced on film, one from each camera. Each resulting photograph contains information in terms of the optical density (grayness) of the developed image which is characteristic of the spectral response of the injured tissue to the imposed illumination. It is the differentiation of these characteristics for the necrosis of tissue at varying depths that allows the ultimate formation and recognition of a diagnostic signature for each category of burn depth.

The methodology is therefore based on the intercomparisons of black and white photographs showing the spectral reflectance of the first few millimeters thickness of the skin. That wavelengths of light in the photographic range can penetrate this depth is obvious when one considers the ability to visually detect certain subcutaneous veins. The reflectance

of these tissues in the visible and the very near infrared spectra (the photographic region under consideration) depends only on the biochemical character of the tissues. Temperature does not become an important infrared factor until one considers the middle infrared wavelengths, typically around 4 μm and 10 μm. A methodology used to measure temperature in this region is called thermography. Since thermography is strongly dependent on the surface temperature, it is susceptible to surface wetness (evaporative cooling), room temperature changes, drafts, thermal equilibration times of the patient, and variations in the state of the peripheral vascular system of the patient. It also requires a quantitative image analysis that includes the weighting of a gray scale or color or color pattern against local temperature to determine an average surface temperature, and the comparison of various average surfaces to indicate deviation from an expected value. Studies conducted during this task on the use of thermography for the diagnosis of burns are discussed in Section V of this report. Additional information obtained by the authors is presented in Anselmo and Zawacki, May 1977. Since the photographic method depends only on the biochemical character of the tissue, no restrictive environmental factors are present. The required image analysis is then quantitative in that the color of the resulting image becomes the actual diagnostic parameter, e.g., blue may denote a shallow partial-thickness injury and red may denote a deep partial-thickness injury.

The formulation of the diagnostic signature is produced by calculating the differences of the optical densities of the three spectral images. The digital values of the grayness of the images are measured from the transparency as a function of the position on the image, and these measured values are then subtracted by the computer for each point of the image and for each pair of original photographs. This process, discussed in Section II, results in three images which are functions of the ratio of the spectral reflectance of the tissue as predicted by Eq. (8).

$$I_1 = I_R/I_{IR}: \text{ red image divided by infrared image} \tag{9}$$

$$I_2 = I_G/I_{IR}: \text{ green image divided by infrared image} \tag{10}$$

$$I_3 = I_R/I_G: \text{ red image divided by green image} \tag{11}$$

There are some practical suggestions that can be made in applying these results to a photographic experiment. The experiment should be conducted by using multiple cameras, placed very close to each other and using the appropriate filter. Simultaneous exposures should be used to obtain a consistent illumination function for all photographs. Consequently, although the geometric factor $Z^*(x',y')$ will not be equal for each exposure, if the cameras are close to each other, their values will vary approximately as the cosine of the angle between the target and the cameras. With lens centers spaced at a distance of 1 ft from each other and with a target distance of 10 ft, there results a difference in values of Z^* of about 10%.

If the photographs are taken in a darkroom by opening the shutters, flashing a strobe lamp, then closing the shutters, the times of exposure for all photographs will be equal,

$$t_{E,i} = t_{E,j} \tag{12}$$

and the source illumination functions will also be equal.

$$i_{0,i}(x',y',T_0,\lambda) = i_{0,j}(x',y',T_0,\lambda). \tag{13}$$

The strobe lamp, however, is not a black body and the integration of the illumination function over different spectral regions will not have a simple functional relationship. However, if the illumination is uniform, the integration of this function over the spectral region of the system bandpass will not vary with position but will be of the form

$$i_{0,i} = \text{const. x } i_{0,j} \tag{14}$$

The transmission characteristics of the camera system $\tau_s(\lambda)$, the filter $\tau_f(\lambda)$, and the sensitivity of the film $S_f(\lambda)$ are complex but easily accounted for since they are functions of wavelength only. After integration they yield a constant value which, for the purposes of this analysis, is not positionally dependent and therefore does not affect the spatial variation in optical density over the image. In order to determine the feasibility of multispectral analysis of burn injuries, the following procedure was used.

The images, I_1, I_2, and I_3 (see Eqs. (9), (10), and (11), were produced as transparencies whose optical density was proportional to the value of the ratios of the parent image spectral reflectances. In these transparencies one can easily recognize the subject of the parent images even though the gray tones may be considerably different.

The image transparencies, I_1, I_2, and I_3, were then used to produce a final image by passing red light through I_1, green light through I_2, and blue light through the photographic negative of I_3, thereby exposing color-sensitive paper. The quantities of red, green, and blue light sum in proportion to the transmission of the exposed images. The resulting color produced on the paper after development is then characteristic of the ratio of the spectral information contained in the bandpass of the filters and of the reflectance characteristics of the injured tissue.

SECTION III

ANIMAL EXPERIMENTS

In order to determine the practicality of this technique, a series of experiments was carried out using experimentally burned guinea pigs. Two limitations were placed on the experiments. First, sample populations were formed whose members exhibited two classes of thermal injuries: partial-thickness skin loss and full-thickness skin loss. Erythema as a class of injury was not specifically considered. Second, the injuries were substantially uniform over the central area of the burn. Although the first condition divided the sample population into only two groups of skin loss, these injuries could not be accurately diagnosed by inspection within the first 2 weeks postburn. The second condition simplified the analytical procedures by limiting the injury to a particular and consistent site for comparison among the animals. The average values of the surface reflectance over this site were then used for the necessary calculations.

Two symmetrical areas of approximately 4 cm^2 each (about 5% body surface area) on the dorsal trunk of 10 white male guinea pigs were clipped and depilated. The animals were anesthetized using IP Nembutal. On one of these symmetrical areas a 75°C, 10-sec scald burn was inflicted using standard technique and apparatus (Walker and Mason, 1968). A second symmetric area of each animal was left uninjured and used as a photographic reference. Five of the animals had their blisters removed by gentle shearing pressure. Previous studies have shown that dehydration from this injury resulting from the removal of the blister leads to full-thickness skin loss (Zawacki, 1974). The remaining five animals had their blisters left intact. This condition results in a partial-thickness skin loss. The injuries were allowed to heal by exposure. Additional trauma was prevented by placing each animal in a separate cage immediately postburn and after each was fitted with an elastoplast trunk binder having a padded aperture surrounding and protecting the burn.

Red, green, and infrared spectrally filtered photographs were taken of the injured areas at 3 min and at 2, 4, 8, 16, 24, 28, 96 and 168 hr postburn. The reflectance pattern over the injured areas was measured from the optical density of the transparencies by a scanning microdensitometer, and the average values were calculated. By using these average values of optical density, the appropriate reflectance ratios were calculated for each injured area. These ratios, forming the values of I_1, I_2, and I_3 (Eqs. (9), (10), and (11)), are plotted in Figure 5. Figures 5a to 5e present reflectance ratio values characteristic of the partial-thickness injury. Note that in all cases one finds the sequence that I_1 is greater than I_2, which is greater than I_3. This appears to be a spectral characteristic of this partial-thickness burn. Figures 5f to 5j show data from animals whose injuries are known to ultimately result in full-thickness skin loss due to dehydration. In these cases the characteristics are such that I_1 is greater than I_3, which is greater than I_2. This becomes the appropriate spectral

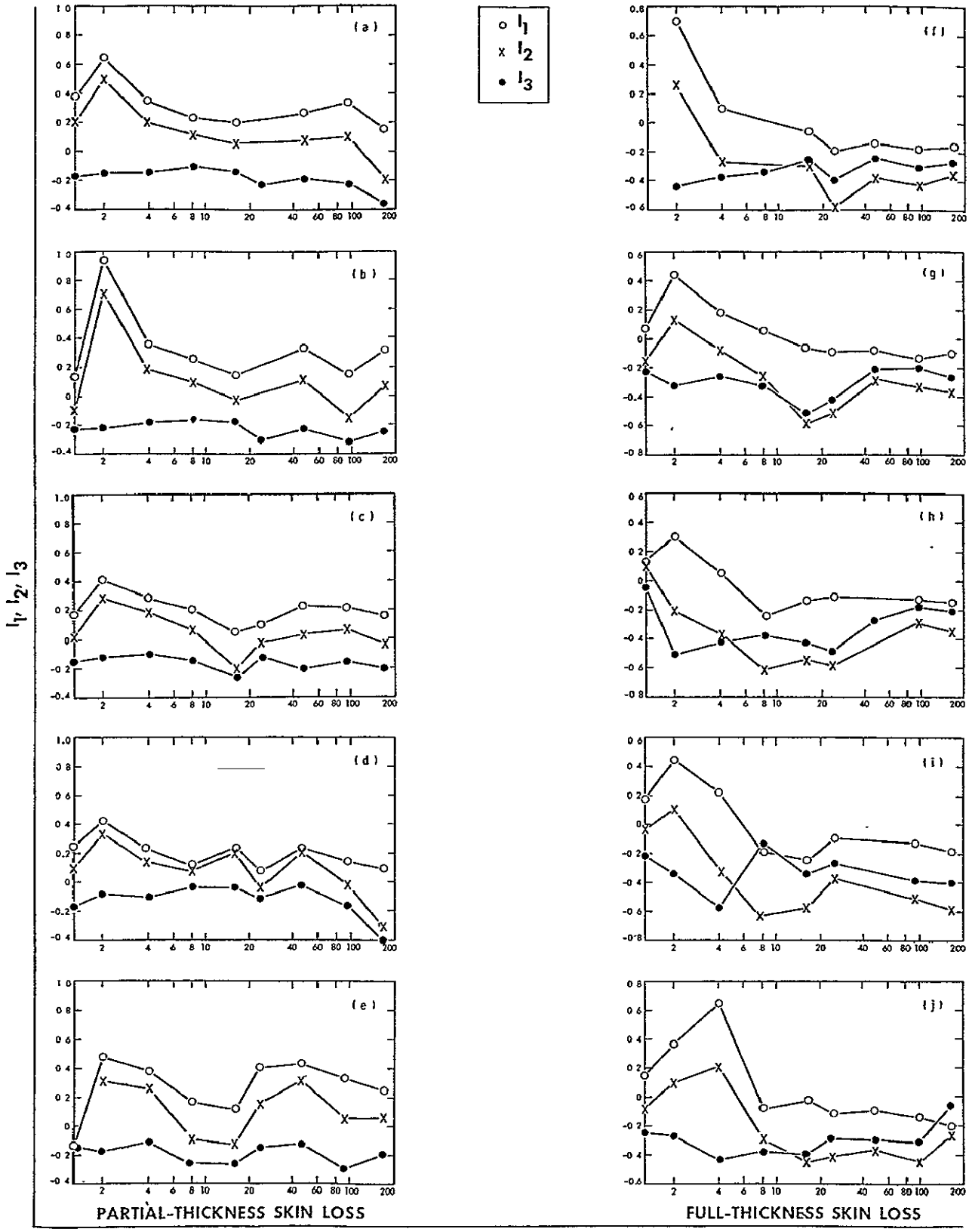

Figure 5. Multispectral Photographic Data from Experimental Burn Site of Guinea Pigs

characteristic for the applied full-thickness injury. It is the characteristic that exists only at later postburn times when the injury is known to be a full-thickness loss. Because it is the relative values of I_1, I_2, and I_3 that would ultimately produce a diagnostic color if exposed to color-sensitive paper as previously described, a major differentiation would occur for these types of burns on the guinea pig. Such spectral characteristics are therefore potentially useful as a diagnostic aid. If it can be shown that the physical processes which produce the spectral characteristics seen in the guinea pig are similar to those which occur in man, this technique could provide an accurate clinical diagnosis for this type of injury about 16 hr postburn or later. It is of considerable interest to note in Figure 5 that the spectral characteristics of injuries of the animals whose blisters were removed and whose injuries ultimately became full-thickness, Figures 5f to 5j, were the same as those of the partial-thickness injuries, Figures 5a to 5e, during the first 4 to 16 hr postburn. This would suggest that the injuries of the second group during the early postburn hours were not yet full-thickness in nature. Evidence exists to support this hypothesis. It has been reported (Sevitt, 1957; Jackson, 1953) that, below the tissue undergoing immediate coagulation necrosis as a result of thermal injury, there exists a "zone of stasis" where progressive microvascular stagnation leads to deepending capillary occlusion (stasis) during the first day or so postburn. In experimental burns produced in the same way as those described above, Zawacki (1974) noted that during the early postburn hours "capillary flow ceased in progressively deeper layers of skin until 16 hr postburn, capillary stasis extended well beyond the deepest hair follicles and almost to the panniculus carnosis." He also noted that, when wound dehydration was allowed, capillary stasis remained full-thickness in depth and was associated with full-thickness skin loss. The nearly simultaneous occurrence of these observations with the change in the spectral photographic characteristics of the injured tissue suggests that the photographic technique is detecting real physical processes resulting from deep capillary stasis and/or dehydration within the tissue, and consequently supports the hypothesis that the technique may be useful as an aid in the early clinical diagnosis of burn depth.

SECTION IV

IMAGE PROCESSING TECHNIQUES

In order to accomplish the photographic analysis discussed in Section II of this report, the facilities of the Image Processing Laboratory (IPL) at the Jet Propulsion Laboratory were used, initially to determine the optimum spectral regions of interest for the burn wound observations and later to develop an image processing protocol. This section presents typical results of the final techniques developed for processing the multispectral photographic images and shows examples of these images.

The color photograph in Figure 6 will be used as an example for discussion purposes. It was taken 21 hours postburn and depicts an injury which is a classic textbook example of the three major zones of burn depth. At the edge of the burn is the red zone of hyperaemia which heals without complication. This is a shallow injury and is not grafted. The center of the injury, the dark brown area of the right chest containing the right nipple, is the deepest injury, the zone of coagulation. This area is definitely destroyed and requires grafting. Between these two areas is the parchment-like region called the zone of stasis. In many cases it is not known whether this area will require grafting or whether it will heal spontaneously. In this case, it was known that spontaneous healing would occur. The example then is a known injury and is appropriate for explaining the image processing methodology.

A close-up view of a section of the mid-chest at 2 hr postburn is shown in Figure 7. Note the width of the zone of hyperaemia and the density of "redness". The same area at 21 hr postburn is shown in Figure 8. Note that the width of the zone has increased and the density of the "redness" has become deeper. The zone of stasis, seen in the upper left corner of Figure 8, also exhibits a deepening in color. These indicate typical changes occurring within the first day postburn and at least partially explain why an accurate multispectral diagnosis cannot be expected until 24 hr postburn. At this time, the changes indicated in Figures 7 and 8 tend to cease, thereby allowing a successful evaluation of the burn depth.

Figure 9 shows the cameras used for the photography. The center camera on the bottom contained the infrared film and filter. The adjacent cameras contained Plux-X film with read and green filters on the lenses. The top camera contained color film for reference purposes. Also shown in this photograph is the optical head of the AGA Thermovision Camera which was used to acquire thermographic data on the burns in an attempt to correlate surface temperatures with the multispectral data. (The thermographic results are discussed in Sections IV and VII.)

The first step in the image analysis process is the acquisition of the proper spectral images. For the burn depth analysis these spectral regions are in the infrared, red, and green. Typical images made from filtered 35 mm transparencies are shown in Figures 10, 11, and 12.

Figure 6. Color View of Injury, 21 Hours Postburn

Figure 7. Close-Up View of Mid-Chest Area,
2 Hours Postburn

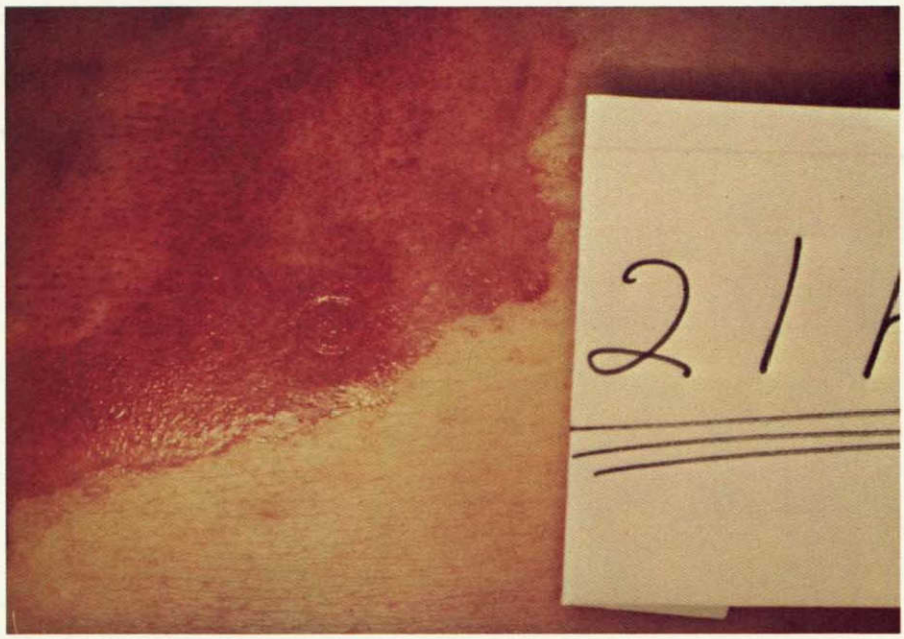

Figure 8. Close-Up View of Mid-Chest Area, 21 Hours Postburn

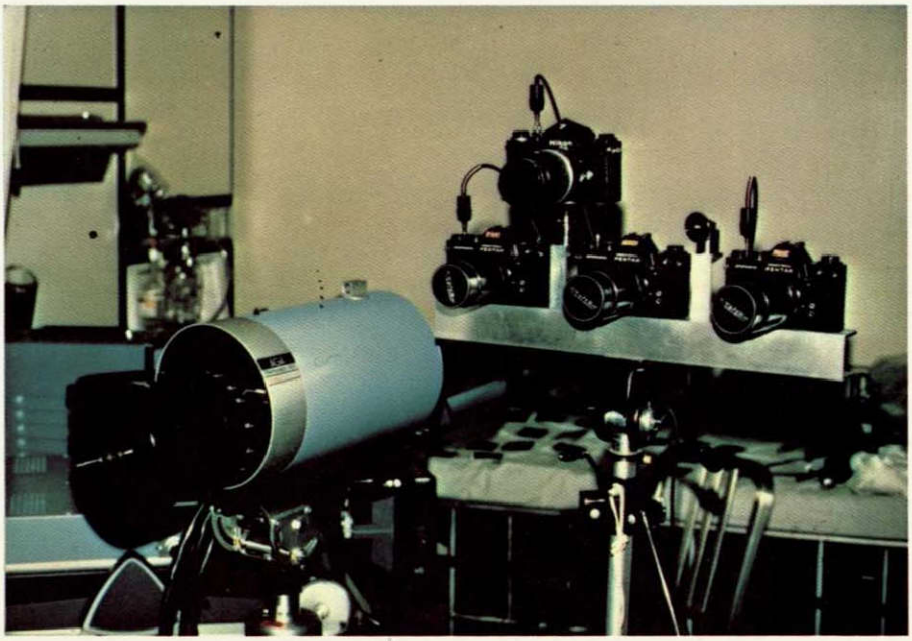

Figure 9. Camera Setup for Multispectral Photography

Figure 10. Infrared Spectrum Image of Burn

Figure 11. Red Spectrum Image of Burn

Figure 12. Green Spectrum Image of Burn

Note the broken appearance of the subcutaneous veins in Figure 10. This indicates thermal denaturation of these veins. Also note the dark, diffuse nature of the areas around these veins. Increased absorptance (darkness) in the infrared appears to indicate thermal denaturation of the vascular system. The diffuse areas of Figure 10 probably indicate the coagulation of the adjacent system, in general implying complete destruction of the skin as shown in Figure 13. The rationale is not that the dermal cells are thermally destroyed in the same manner as the vascular system but that, since the vascular system has been destroyed, the dermal cells have lost their nutrient supply, as have the hair follicles and sweat glands, thereby preventing the injury from spontaneously healing from below. In cases of small area coagulation, healing may result by migration of cells from the periphery of the injury; however, this case is of minor importance for most injuries greater than a few square centimeters. Finally, the general appearance of the thermal injury presented in Figure 10 bears a remarkable resemblance to that shown in Figure 4, in that the vascular system has taken on the appearance of broken and isolated sections, as opposed to the more continuous vessels expected from experience.

Figure 11 presents a photograph taken in the red spectrum. In general it would be expected that red surfaces, such as hyperaemic areas and skin containing a normal perfusion of oxygenated hemoglobin, would appear "bright" in the image. That such is the case can be seen by

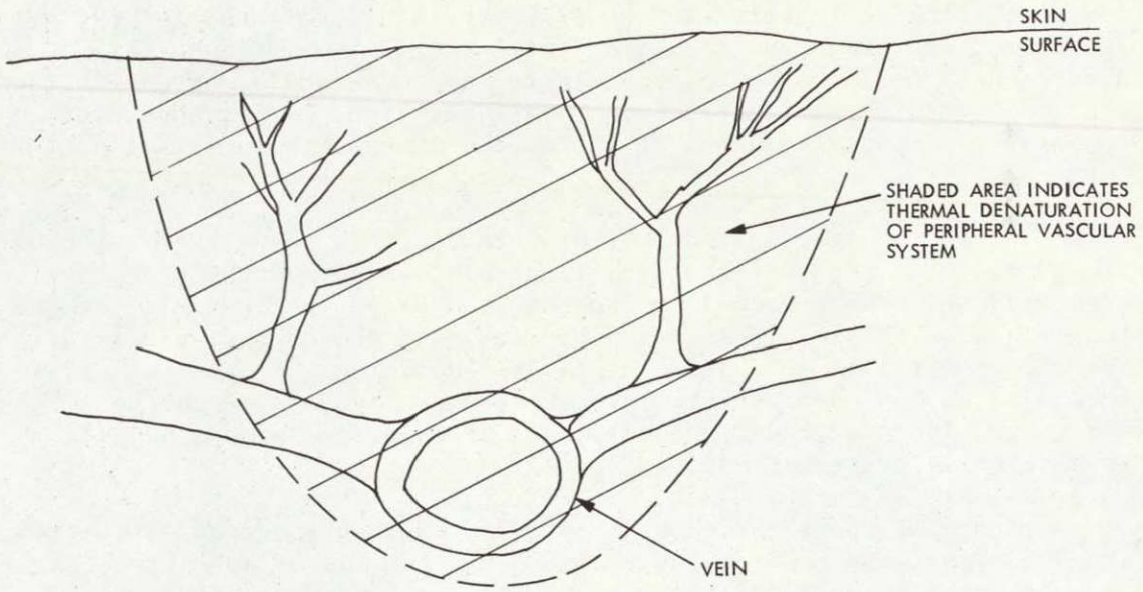

Figure 13. Interpretation of Damage Indicated by Increased Infrared Absorption (Figure 10)

comparing the central chest area in Figures 6 and 11. Other conditions such as regions of increased venous blood concentration, and possibly thermally denatured blood, would be dark (high absorptance). Once again a comparison of Figures 6 and 11 shows this to be true. Further comparison between Figures 10, 11, and 13 implies that the more diffuse character of the dark area of Figure 11 is due to the superficial thermal damage in the area of deep burn and the specification of these areas by investigation in the red spectrum.

Figure 10, the infrared data, appears then to indicate thermal damage of the vessels at the deepest levels of the skin as described in Figure 13. Figure 11 includes additional information concerning thermal damage in the more superficial areas of skin, again as indicated in Figure 13.

The image depicted in Figure 12 was taken in the yellow-green spectrum. In this region, areas of coagulated or deoxygenated blood as well as hyperaemic zones appear dark, thereby leaving the zone of stasis, the area of reduced perfusion, as the lighter region. This region can be seen as the lighter surface on the mid-area of the right chest. The major work of the analysis is the determination of the severity of the injury to this zone. Because these zones do not always appear dark or light as shown in this example the only accurate analytical approach is

accomplished by noting the relationship of the spectral reflectance on the unknown zone to that of the zones of hyperaemia and coagulation. For example, consider the data of Table 1, which is taken from this example study. On each area of the image a subjective evaluation of the surface reflectance is made as to whether the reflectance is low, moderate, or high relative to the distributions within the injury. Therefore, the green spectral image yields a low reflectance (high absorptance) in the zones of coagulation and hyperaemia whereas in the zone of stasis the reflectance is relatively high. It is the inter-comparison of these values that yields the diagnostic information of interest.

The second step in the analysis procedure is the digitization of the images, the production of the image histogram, and the construction of a grid network on each image so that the proper registration of the images can be obtained. An example of this is shown in Figure 14 with the red spectral image. Grid points are chosen so that the red and green images can be translated, rotated, and warped to match the infra-red image within a predetermined area. In this case study, only the area of the right chest was registered.

Figure 15 shows the results of a contrast enhancement of the red image of Figure 14. Using the red image as the fixed image, the infra-red and green images were then translated, rotated, and warped to register with the red image at five locations on the right chest. Five points provide adequate registration with a minimum of computer time. The registered and contrast-enhanced infrared and green images are shown in Figures 16 and 17, respectively. To observe the results of contrast enhancement, compare Figure 16 with Figure 10, Figure 15 with Figure 11, and Figure 17 with Figure 12.

The third step in the analysis process is the formation of the inter-ratios of the three image reflectances. Equation (8) shows that in order to form the ratio of the surface reflectances as taken from a photograph, the image optical densities must be subtracted. This was accomplished on the computer and the results are shown in Figures 18-20.

Table 1. Reflectance Trends for Zones of Burn

	Zones of Burn		
Spectral Region	Coagulation	Stasis	Hyperaemia
Infrared	Low	Moderate	Moderate
Red	Low	High	High
Green	Low	High	Low

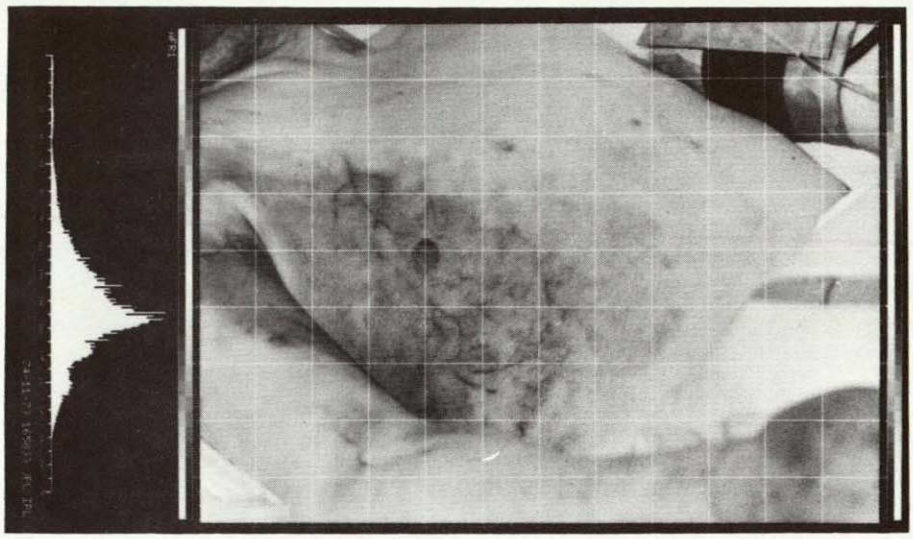

Figure 14. Print from Digitized Red Image With Histogram and Grid (for Registration)

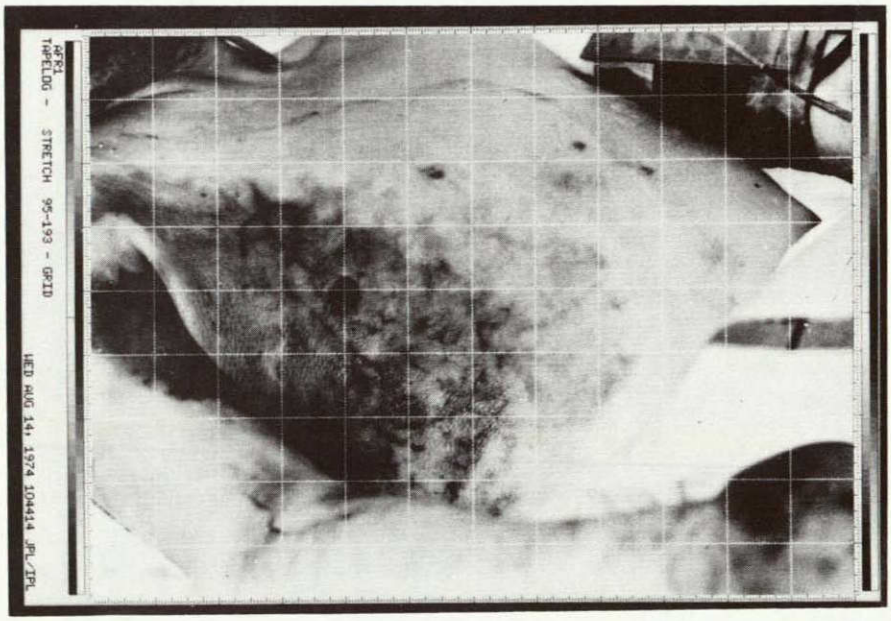

Figure 15. Contrast-Enhanced Red Image

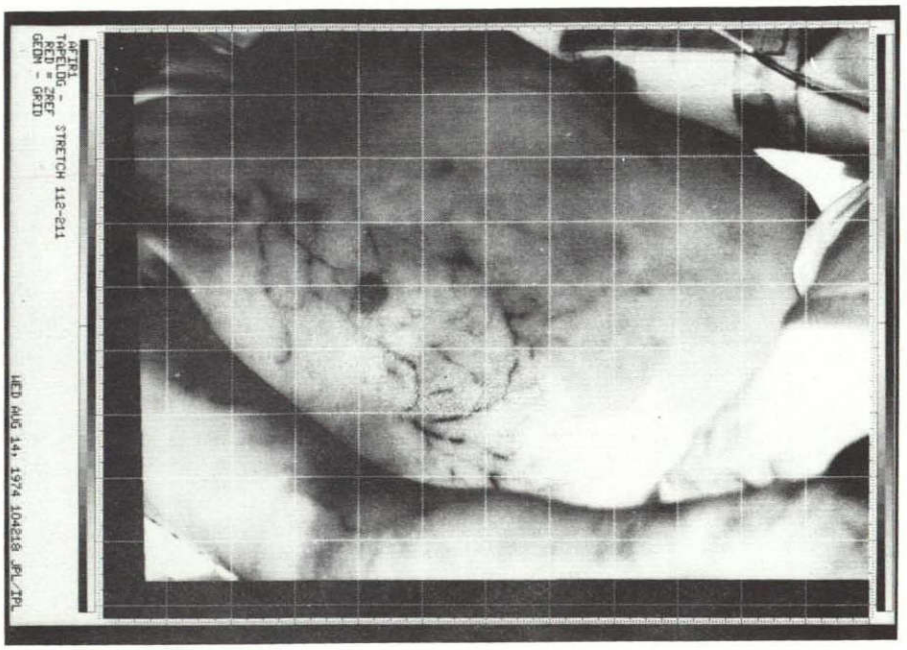

Figure 16. Infrared Image with Contrast Enhancement and Registration

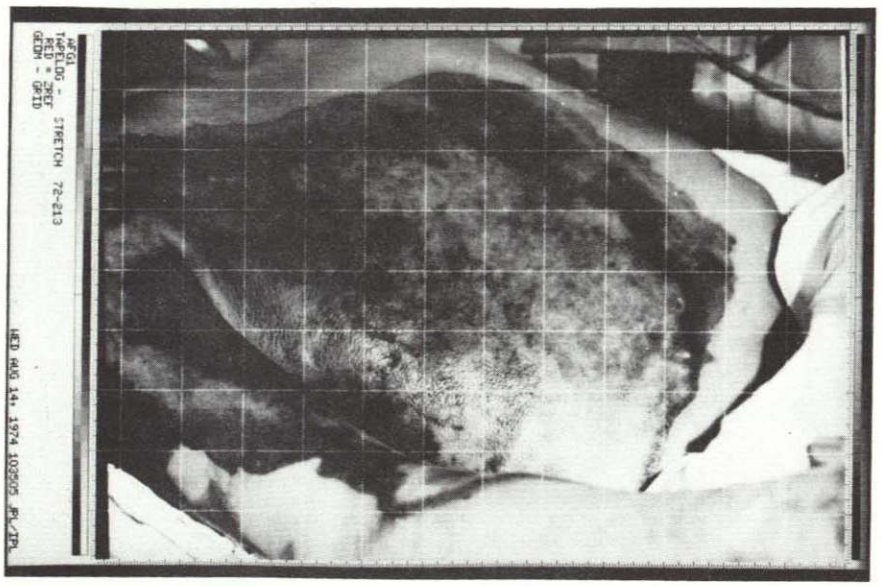

Figure 17. Green Image with Contrast Enhancement and Registration

Figure 18. Infrared Minus Red Image: ρ_{IR}/ρ_{RED}

Figure 19. Infrared Minus Green Image: ρ_{IR}/ρ_{GREEN}

Figure 20. Red Minus Green Image: ρ_{RED}/ρ_{GREEN}

Figure 18 is the infrared minus the red image, forming the ratio of the infrared to the red reflectance of the skin; Figure 19 is the infrared minus the green image, forming the ratio of the infrared to the green reflectance; and Figure 20 is the red minus the green image, forming the ratio of the red to green reflectances.

The pattern recognition logic for the identification of the burn characteristics can now be considered. Table 2, column A, presents the ratios of the reflectances as assigned to each burn zone of the image for each spectral region from Table 1. The general categories of values are assigned as high, medium, or low. The ratio of the infrared to red reflectance in the zone of coagulation yields the ratio of two low numbers. The magnitude of this ratio will be of the order one, O(1). The same ratio in the zone of stasis results in the ratio of a medium to a high value, which is of the order one-half, O(1/2) (with normalization).

Table 2. Reflectance Ratio Trends for Zones of Burn

Reflectance Ratio	Color Assignment	Zones of Burn								
		Coagulation			Stasis			Hyperaemia		
		A	B	C	A	B	C	A	B	C
ρ_{IR}/ρ_{RED}	Red	L/L	O(1)	H	M/H	O(1/2)	M	M/H	O(1/2)	M
ρ_{IR}/ρ_{GREEN}	Green	L/L	O(1)	M	M/H	O(1/2)	L	M/L	O(2)	H
ρ_{RED}/ρ_{GREEN}	Blue	L/L	O(1)	L	H/H	O(1)	L	H/L	O(3)	H
		Yellow			Red			Blue		

L = low; M = moderate; H = high

A similar value occurs in the zone of hyperaemia. Continuing this logic, column B of Table 2 is formed for each zone and for each reflectance ratio. Next the intercomparison between zones must be made for each ratio. The maximum order of the reflectance ratio for the infrared to red data occurs at order one. This is assigned a high value of optical density (H) for the resulting image. Since a minimum value of zero would occur for a ratio of (L/H), the image area having a reflectance ratio of O(1/2) would result in a mid-range (M) optical density value. These values are noted in column C of Table 2. Similar logic is used for the infrared to green ratio. The maximum ratio of order 2 assigns a high value to the optical density in the zone of hyperaemia. Then it follows that order 1 assigns a mid-range value to the zone of coagulation and a low value to the zone of stasis. In a similar manner for the red to green ratio, the maximum value of order 3 assigns the high brightness value to the zone of hyperaemia and low values to the other zones.

In the analytical protocol, the images composed from the three reflectance ratios are formed to produce a diagnostic image by assignment of each ratio to a color, which is then added, either to form a final image on color sensitive photographic paper or, as will be discussed in Section VI, on a color television monitor. The image formed by the ratio of the infrared to red reflectance is assigned to RED; that formed by the ratio of the infrared to green is assigned to GREEN; and that formed by the ratio of red to green is assigned to BLUE. The resulting characteristic of each zone of injury is then produced by the addition of light quantities in the ratio indicated by the magnitudes given in column C of Table 2. The zone of coagulation has high and medium quantities of red and green light with little blue; the addition of these quantities of light results in a "yellow" characteristic color. The zone of hyperaemia yields a blue or cyan characteristic due to the small amount of red light added. The zone of stasis results in a red color due to the small amount of green and blue light added. These are the results which are obtained in the final pseudocolor diagnostic image as shown in Figure 21. The blue area at the edge of the burn on the upper right and mid-chest is the characteristic color of a partial-thickness injury which will heal spontaneously. The red area adjacent to this injury is the deep partial-thickness injury. This will heal but may result in serious scarring. The right lateral chest area which contains yellow, white, and light blue is the full-thickness injury and will not heal spontaneously. The white and light blue are present because of the high intensity of blue light imposed on the photograph during processing (at an early time in this study). It is readily apparent that should the blue intensity be decreased, these areas would all become yellow. Yellow is the characteristic color presently used for the prediction of full-thickness injury. The basic color diagnostic scheme using this technique is as follows.

Burn	Characteristic Color
Full-thickness	Yellow, yellow-green
Deep partial-thickness	Red
Partial-thickness	Blue

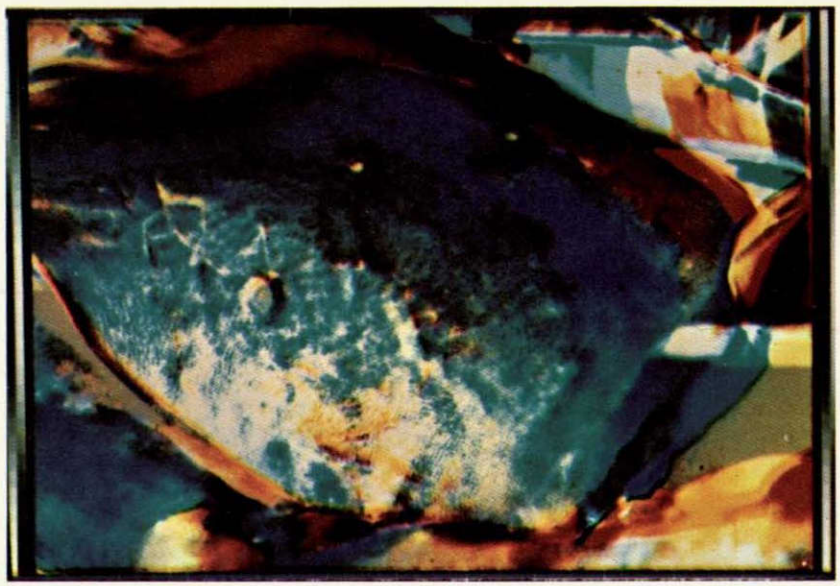

Figure 21. Pseudocolor Diagnostic Image

Since the burn injury usually occurs as a complex mixture of full and partial-thickness injury, it often is necessary to interpret the meanings of mixed color areas. For example, an area that has both red and blue is interpreted as an area of partial-thickness injury but the amount of the deep injury is estimated by the percentage of the area containing red. In some cases, all tissue showing deep partial-thickness burns will be removed to allow minimum scarring on a face or hand; in other cases, as on the back of an adult, it may cause no problems if allowed to heal with time. Cases in which the image contains yellow and red, indicating mixed full- and deep partial-thickness burns, may be allowed to heal only if the red and yellow are present on a very large burn area where each cm^2 of viable tissue could be important in the healing process; on small burns, these areas would probably be removed and grafted. Therefore, the case of mixed burns poses no real problem to the multispectral diagnostic process but involves normal decisions always considered by the physician. With the multispectral data, however, the physician has an early and accurate diagnosis to support these decision processes.

SECTION V

RESULTS OF CLINICAL PHOTOGRAPHIC ANALYSIS

During the final phase of the photographic study, 68 burned areas on 12 patients were analyzed using the multispectral approach.* The results of this study are presented in Table 3. Thermographic data were obtained on some of the patients to permit a comparison of the methodologies. The results are included in Table 3. In order to determine an accurate final diagnosis of the burn injury, two approaches were required. If the patient was not grafted, the natural healing process of the injury was used to determine which areas healed (partial-thickness injury) and which did not (full-thickness injury). If the patient was grafted prior to accurately establishing the depth of injury, the depth was defined by the judgement of the surgeon following the grafting procedure. In these cases the surgeon can often make a reasonable estimate of the depth of injury once he begins to remove the necrotic tissue on the surface of the injury.

Although not all of the complicated small areas and structures involved in burn injury could be classified on an objective basis, 100% of the cases studied using the multispectral imaging method presented correct subjective diagnosis of the depth of injury as early as 21 hours after the injury for cases which could not be diagnosed with certainty by the surgeon. Some examples of these case studies are presented in Figures 22-24. Figure 22 shows a 2-1/2 year old white male who experienced hot coffee scald burns. The conventional diagnosis upon admission was 15% total area burns with no third degree injury. The multispectral analysis and the thermogram were made one day postburn. The blue diagnostic color of the multispectral image indicated partial-thickness burn and supported the physician's original diagnosis.

It is of interest to note that this patient was treated with topical sulfamylon cream which was not removed from the surface prior to taking the photographs. The ointment did not affect the multispectral

---

*Earlier patient studies leading up to the development of this analytical approach, the selection of proper spectral filters, the use of multispectral comparisons, and pseudocolor presentation techniques are considered of no value to this report and are not included. In summary of this early work it can be said that the enhancement of the infrared image gave the most information on identifying the large percentage of full-thickness burns but provided no information on the other classifications. Extensive studies in the use of high and low pass digital filtering, contouring, and other mathematical relationships of the surface reflectance did not identify techniques that would be competitive with those presented in this report; however, the results of these studies may be useful in the future in developing methods for the enhancement of the final pseudocolor image. These techniques will be discussed in Section VI.

Table 3. Results of Clinical Photographic Analysis

Patient	Area	Final Diagnosis	Agreement With Final Diagnosis		
			Days Postburn	Multispectral Correct?	Thermography Correct?
A	Chest	Full-thickness	1	Yes	Yes
			2	Yes	Yes
			3	Yes	No
B	Left and right legs	Full-thickness	1	Yes	(No Data)
			5	Yes	
			7	Yes	
			8	Yes	
C	Chest, right arm	Mixed	1	Yes	(No Data)
			5	Yes	
			8	Yes	
D	Chest	Mixed	1	Yes	(No Data)
			3	Yes	
			13	Yes	
			19	Yes	
			22	Yes	
E	Chest, left arm	Full-thickness	1	Yes	(No Data)
			3	Yes	
F	Chest	Partial-thickness	1	Yes	No
			2	Yes	No
			7	Yes	Yes
			8	Yes	Yes
			9	Yes	Yes
			10	Yes	Yes
G	Back	Partial-thickness	1	Yes	(No Data)
H	Back	Partial-thickness	1	Yes	(No Data)
I	Chest, left arm, left hand	Mixed	1	Yes	No
			2	Yes	No
			3	Yes	No
			5	Yes	No
			6	Yes	No
J	Chest	Full-thickness	1	Yes	(No Data)
K	Chest	Mixed	2	(No Data)	No
			9		No
			16		No
L	Chest	Partial-thickness	1	Yes	No
			2	Yes	No
			3	Yes	No
			4	Yes	No
			5	Yes	No
			12	Yes	No
M	Chest, right and left legs, abdomen	Mixed	1	Yes	Yes
			2	Yes	Yes
			3	Yes	Yes
			7	Yes	Yes

a. Color Print of Burn

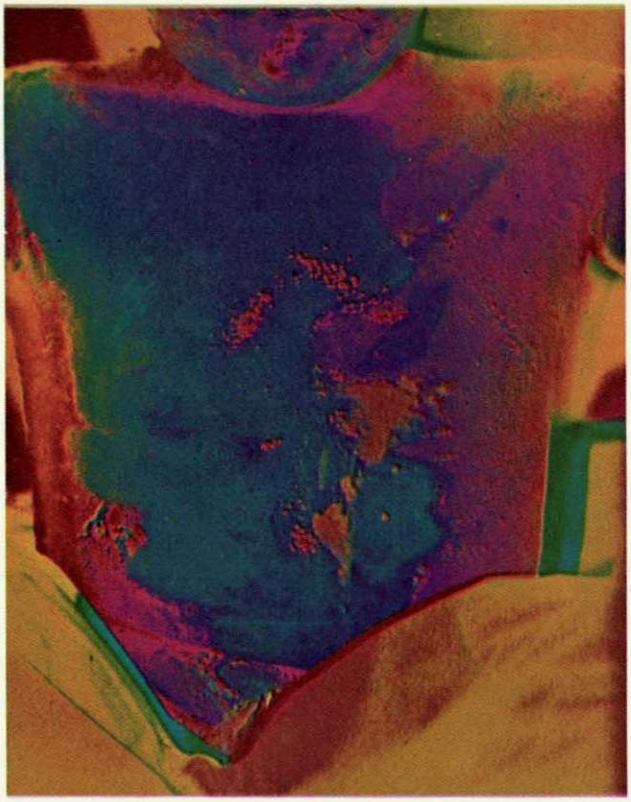

b. Multispectral Analysis

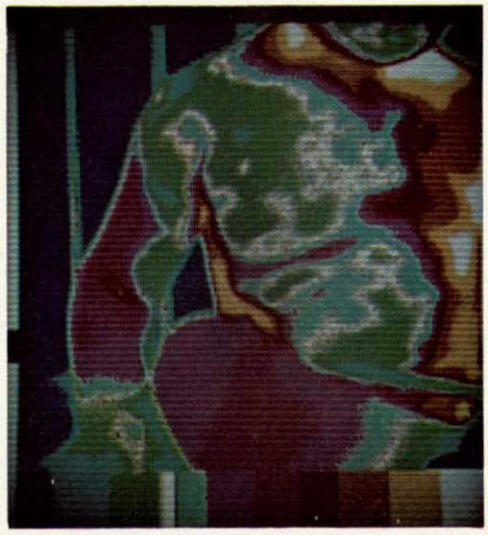

c. Thermogram

Figure 22. Partial-Thickness Injury

a. Color Print of Burn

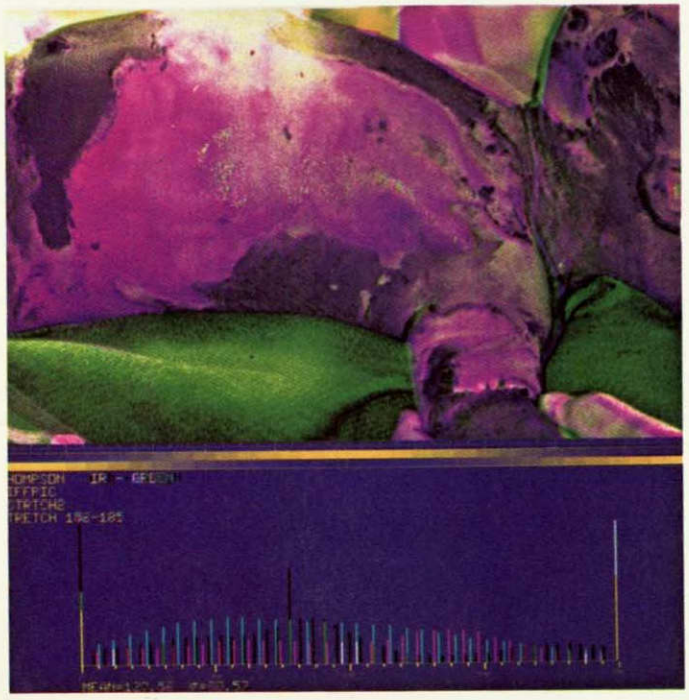

b. Multispectral Analysis

c. Thermogram

Figure 23. Deep Partial-Thickness Injury

a. Color Print of Burn

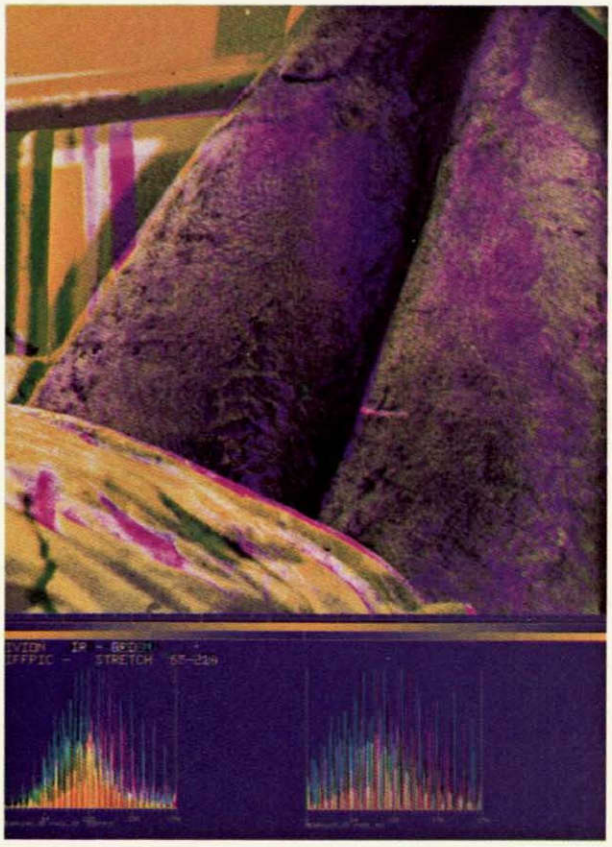

b. Multispectral Analysis

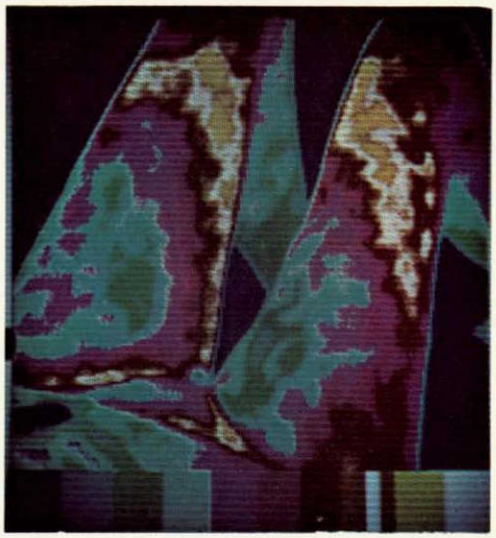

c. Thermogram

Figure 24. Mixed Depth Injury

In this study thermography was used to gain insight into the thermodynamic nature of the burn wound. It was initially felt that this insight could be useful in the application of the multispectral diagnostic procedure. It has been shown, however, that the multispectral method is able to accurately predict burn depth by direct use with a physician. Thermography, on the other hand, may still have a role in burn diagnosis. The study reported here identified potential problems with its use but, owing to a lack of resources, did not undertake to solve these problems.

SECTION VI

THE MULTISPECTRAL IMAGING SYSTEM

A. SYSTEM REQUIREMENTS AND DESIGN

In designing an automated imaging system, the objective was to preserve the mathematical functions of the photographic methodology while eliminating the complicated, time consuming, and expensive processes of that method. Consequently, photodetectors were chosen as sensors so as to allow direct access to automated computer analysis. This greatly reduces the length of time required for the production of a diagnostic image. Three spectral channels of simultaneous data could be made available by using three detectors, each with its own filter. Image construction could be accomplished by the use of a scanning mirror. With three separate detectors, registration problems could be solved by mechanical positioning of the sensors. From practical experience, it was determined that an exposure time of one-half second or less would be adequate for patient positioning. With a minimum picture format of 128 x 128 6 bit pixels, there would result 98,304 bits per picture, 294,912 bits for 3 pictures, or a data rate of 589,824 bits per second. Also from practical experience, it was decided that a 20^{o} field of view would be appropriate for most of the burn injuries seen in the clinic or hospital, and would allow a reasonable working distance between the patient and the camera.

Image display requirements included the ability to display both monochromatic representations of each of the spectrally filtered digital images, and color representations of each set of three images by assignment of a digital image to a red, green or blue input of an RGB color monitor.

General analytical programming requirements include the ability to present a brightness histogram of each individual image and to determine from that histogram the parameters necessary to apply a linear stretch contrast enhancement to the image. A monochromatic display of the stretched image would allow the appropriateness of the stretch to be determined. The requirement for producing the three inter-ratios of the target surface reflectances could be met by division of the appropriate data numbers for each pixel element of the two images since the photodetectors can be operated so as to produce linear transforms between target brightness and data numbers. It is often necessary to form the inverse of each image, that is, the image formed by setting black to white and white to black.

A total processing time constraint of a few minutes is imposed to allow retaining the unbandaged patient so that the attending physician can simultaneously inspect both the diagnostic image and the injury. This allows further analysis of questionable data or continued analysis of other areas should it be desirable.

Long term data storage is required so that the instrument may be turned off and the data recovered and displayed again at a later time. In cases where new analytical or pathological information is gained, it would also be a requirement to reintroduce and analyze older data in terms of current information.

Some measure of portability is needed. This requires that the imaging camera be separate from the basic electronics and display consoles, and that the entire system can be moved easily between rooms on a given floor or to an elevator for transport between floors.

Stringent requirements to eliminate electrical shock hazards are a necessity. In general, the system will be required to operate in room environments of up to 27°C for extended periods of time.

In addition to these requirements, general goals of flexibility in the choice of spectral regions within the visible and very near infrared, and in the choice of algorithms used for analysis are desirable for the system. These goals provide the potential for simple analytical improvements and for consideration of applications of the system to other medical diagnostic problems. Table 4 summaries these functional requirements.

Table 4. Medical Camera Functional Requirements

Three-color camera - simultaneous and registered
Spectral bands at 550, 620, and 800 nm
Exposure time $\leq$0.5 sec
Format: 128 x 128 minimum
Field of view: 20°
Monochrome display each channel
Histogram, stretch, inverse each channel
Ratio of channel pairs
False color display of ratios
Total processing cycle = few minutes
Long-term data storage
Flexible (other filters, other algorithms)
Portable (with assistance)
Clinical safety

In defining the camera system the first major decision was to use a digital approach. Digital equipment and expertise in digital systems were available at JPL; consequently, there was a strong bias in that direction. It also appeared that the required analytical processing could be carried out more easily and accurately using a digital approach. The flexibility of the digital approach (as exemplified by the potential for continual software changes to allow updating of analytical techniques and the introduction of new algorithms) made this approach quite attractive. A second major decision concerned the trade-off between hardware and software in the processor. Implementation of the various processing functions in a hardware function appeared to limit future changes and potential new applications for the system. Consequently, a more general processor operating from software instructions was chosen. This approach appeared both to minimize the number of parts necessary to do a relatively complex processing task and to provide a potential for the analytical flexibility necessary for continual updating and future growth of applications.

The electronic camera system which emerged from the design effort is described in the following sections. This description is presented in terms of three subsystems. The first is the camera head, the system which acquires the three spectrally filtered and registered images. The second is the digital processor, built around a microprocessor and its associated memory. The bulk of the analytical work is accomplished in this subsystem. The third consists of the software which controls execution of the analysis and central processing of the data.

B. CAMERA HEAD

The camera head is a single piece of equipment with a volume of approximately one-half cubic foot. It is mounted on a tripod for portability. Its task is to acquire three channels of spectrally filtered simultaneous images and to deliver these images in proper format to the video processor. Figure 25 is a block diagram of the camera head system, and Figure 26 is a photograph of the same. The basic signal flow through the system will be discussed. Detailed descriptions of each element are then presented.

Light entering the camera head through the objective lens is passed by a scanning mirror through the field lens to a beam splitter system. The first beam splitter reflects one-third of the incident light and passes two-thirds. The second beam splitter reflects one-half of its incident light and passes one-half, thereby supplying each sensor channel with one-third of the entering light.

After passing through the appropriate filter, each sensor, with gain set by its own amplifier, sends its signal to be multiplexed on a pixel by pixel basis, sampled and held for the 10 bit analog to digital converter and conditioned through the buffer to a video processor.

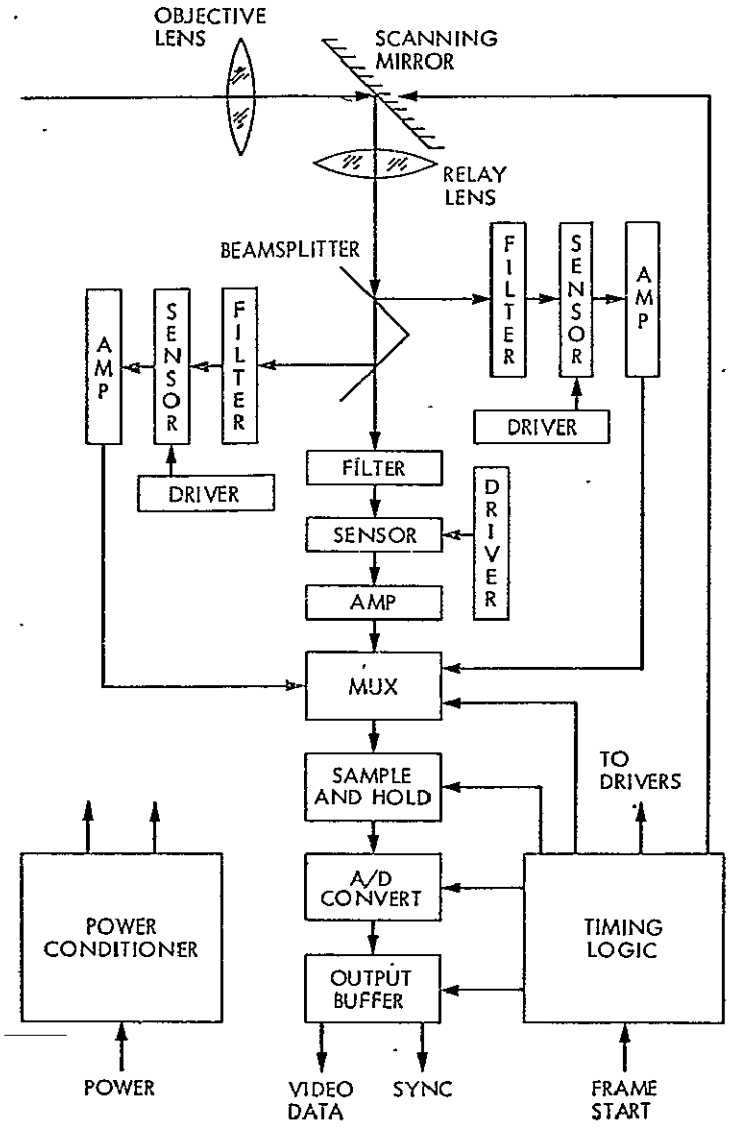

Figure 25. Block Diagram of Camera Head

1. Lenses

Cost and time constraints led to the decision to utilize commercially available lenses. The requirement for the beam splitter determined the type of optical system used. With a field of view of 20^{o} and an array of detectors 13 mm in length, an objective lens with a focal length of 35 mm was necessary. The size of the beam splitters and the requirement to place spectral filters between the lens and the individual sensors required an objective lens with a back focal length of 105 mm. Consequently a relay system was decided upon. A one to one relay system was chosen so that the image produced by the relay lens would fall two focal lengths behind the relay lens. The problem of producing a properly illuminated image with a relay system was recognized; however, the Reticon sensors are positioned to see only the center one-third of the field of the lenses. In the final design the field

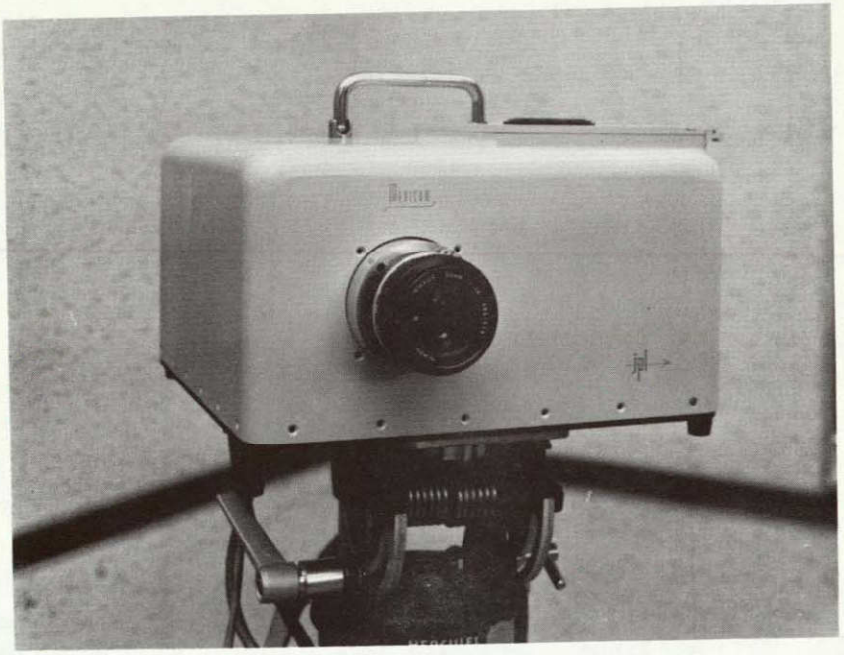

a. With Cover

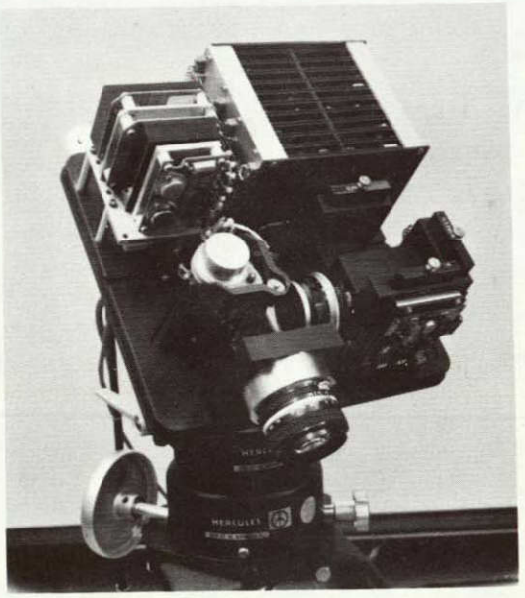

b. Optical Path and Electronics

Figure 26. Camera Head

lens chosen was a 35 mm F1.4 Nikor and the relay lens was a 50 mm F2.0 Nikor. Although the combination was chosen for best illumination of the sensors, the resulting performance showed that some vignetting still occurred at the initial and final scanning edges of the image. This problem has been minimized by utilizing a 50 mm F1.2 lens and developing a softwear calibration correction.

2. Scanning Mirror

The scanning mirror is a plane first-surface mirror mounted on an AC synchronous motor. The exact scanning rate is achieved by a gear reduction device. The command to scan is given by a signal from the operator which is conditioned by the timing logic circuit.

3. Filters

The three filters chosen for the burn diagnosis application were selected to be used with the silicon diode sensors in such a way as to approximately duplicate the transfer characteristics of the photographic system previously used. The first is a band pass filter centered at 550 nm with a nominal band width of 15 nm. The second is a band pass filter centered at 620 nm with a nominal band pass of 15 nm. The third is a Schott RG9 filter. These filters, purchased from Melles Griot, are 2 x 2 inches and are held in special removable frames so that they can be interchanged with filters of other characteristics if required. The spectral response curves calculated for the combination of filter and silicon photodiode are shown in Figure 27. An exact match between this system and the photographic system was not easily attainable within budgetary constraints. The primary disagreement is in the infrared channel, where a wider spectral response is available from this system than from the photographic system. From the results of preliminary tests, this does not appear to be detrimental for the purpose of burn depth diagnosis.

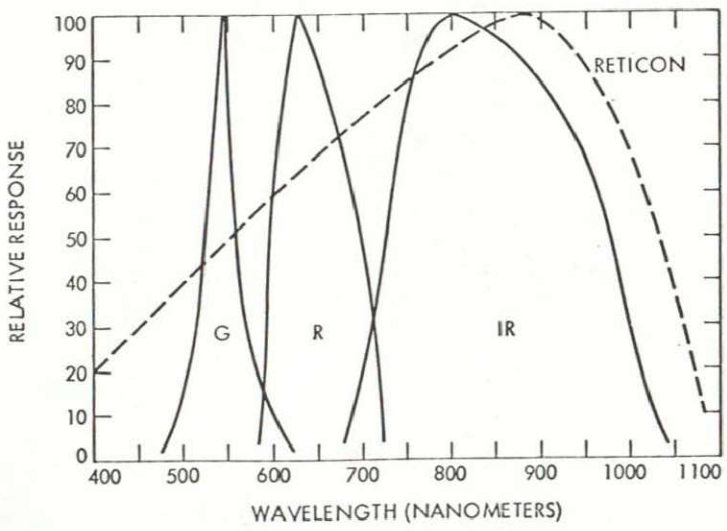

Figure 27. Spectral Bands for Burn Wound Analysis

4. Sensors

With a requirement for spectral response from 500 to beyond 800 nm, silicon sensors were considered. Silicon target vidicons, charge-coupled devices and silicon diode arrays were potential candidates. The need for registered images placed a severe requirement on raster stability, thereby eliminating the silicon target vidicon. The decision to choose the diode array was made on economic grounds, the charge-coupled devices being considerably more expensive at the time. The sensors chosen were the Reticon Line Array, #RL512c. These are linear arrays of silicon photodiodes, each array containing 512 diodes. This array device was responsible for introducing the scanning mirror to the system. With 512 elements available and a minimum requirement for a 128 line system, the signals from four adjacent diodes are summed prior to digitization of the data. This procedure had the effect of not only producing the required 128 lines but also of increasing the signal-to-noise ratio for each line.

5. System Focus and Registration

The registration of the sensors is accomplished mechanically with six degrees of freedom available at the sensor. Position and rotation in the focal plane is accomplished by means of oversized mounting holes connecting the sensor board to the camera case. The focus position and rotation normal to the focal plane is accomplished by the use of shims. Separate focusing of the relay and objective lenses is possible because they are separately and independently mounted.

Various spectral filters result in different path lengths for the relay system and consequently in slightly different magnifications of the three spectral images. With the filter system used for the burn diagnosis problem, this difference is barely noticeable, being less than one pixel in 128.

6. Sensor Drivers and Gain Adjustment

The sensor drivers were also obtained from the Reticon Corporation and were used with only slight modifications to the boards in order to slave two driver boards to the third. This allows the three to operate synchronously.

Separate amplifiers for each sensor allow the gains to be set in an individual manner and according to the filter system used. This allows a relatively uniform brightness level for all three channels and assures proper operation of the sensors. Of the three channels, the infrared produced the strongest signal because of the good match between the spectral filter and the response characteristics of the silicon diodes. The gain of the infrared channel was set so the RMS noise was approximately equal to one-half of one gray level of the digital system. The other channel gains were adjusted to give approximately the same signal strength.

7. Timing Logic

The timing logic synchronizes the functions of all elements in the camera head. Although the sensors are constantly in operation and being read, data are not sent to the video processor until a "Take" command is manually presented by the operator. When this "Take" command is given, the video processor is prepared to accept data and a frame start signal is provided through the timing logic. This activates the scanning mirror which scans through one frame and also initiates the transfer of one frame of data from the output buffer of the camera head into the digital data processor.

8. Camera Head Interfaces

The camera head interfaces with the digital electronics include a 110 volt 60 cycle line brought on a separate line to minimize electrical cross talk. The frame start signal is initiated by the operator with a "push button" switch. This signal starts the rotation of the scanning mirror and causes one frame of three-color data to be transferred out of the camera into the video processor. This parallel bit stream of video data, coming from the three spectral channels and multiplexed on a pixel by pixel basis, contains one set of three spectral frames, each having 128 x 128 picture elements per frame. This three-color frame is transferred in 0.5 second, equivalent to a line time of 1.3 milliseconds. The equivalent pixel time is 10 microseconds and the equivalent bit rate is 1.7 microseconds.

C. DIGITAL PROCESSOR

The digital processor occupies two 4-foot electronics racks and is connected to the camera head by 20-foot cables. Figure 28 is a block diagram of the processor in which the camera head is shown as one of the peripherals. Figure 29 is a photograph of the digital processor racks.

The processor accepts a three-color picture from the camera by a preparatory software statement and a manual command of the operator with a "push button" device attached to the camera head. A three-color picture is then loaded through the direct memory access channel into a predetermined address section of the random access memory (RAM). When the frame has been loaded into the RAM, control of the system transfers to the software located with the microprocessor. Through software commands, stored data may also be entered via the direct memory access channel from the digital tape recorder.

Software control for various analytical and housekeeping functions is possible through the keyboard terminal and both monochromatic and color display of the stored digital images can be brought to the color monitor or stored on the digital tape recorder.

Programming of the microprocessor can be accomplished either by an automatic function from the programmable read only memory (PROM), by

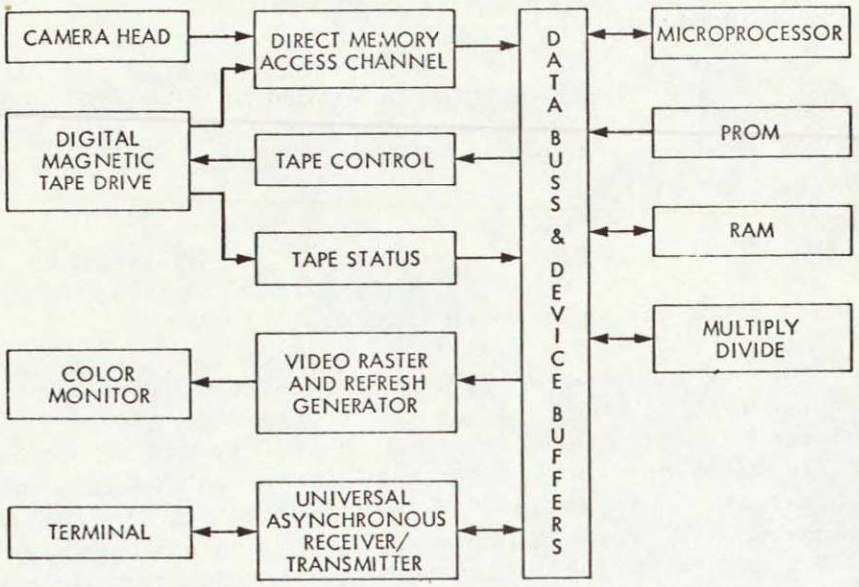

Figure 28. Block Diagram of Processor

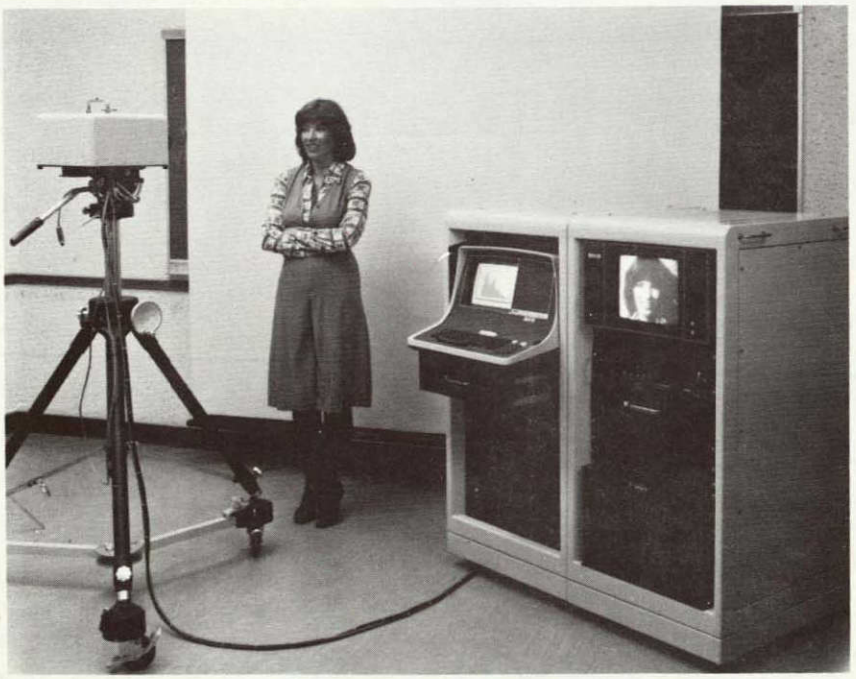

Figure 29. Processor Racks with Camera Head

various programs stored on magnetic tape through the digital tape recorder and the direct memory random access channel, or by direct input through the terminal editing functions.

1. Processor Hardware

The digital processor is designed around an RCA-1802 COSMAC microprocessor. This microprocessor was chosen because of its availability and because of in-house experience with the device. The 1802 has 16 bits of address capability.

The programmable read only memory (PROM) is an Intell erasable PROM, part #2708, with a storage capacity of 1024 by 8 bits. Six of these erasable PROMS are used in the microcomputer.

The random access memory (RAM) is from Monolithic Systems Incorporated of Englewood, Colorado. It is built on metal oxide semiconductor (MOS) technology and although its speed is useful, its organization of 112,000 12 bit words does not directly meet the requirements of the processor for 6 and 4 bit words. The access time for the RAM is less than 500 nanoseconds. Periodic refreshing of each memory location is required. This takes an additional 500 nanoseconds every 30 microseconds but can be postponed for short periods of time. Consequently, it is necessary to either control the refresh cycle selection or to use a slower access time of approximately 1 microsecond. This would increase processing time by a factor of 2.

To minimize this process time, a hardware multiply and divide module is used to accomplish those functions. The multiply-divide module is a Gnat 8005 module from Gnat Computers of San Diego, California.

The digital magnetic tape drive, a Cepher Model 85H, comes from Cipher Data Products Corporation of San Diego, California. It is designed for use in data acquisition and computer processing systems where data must be acquired and stored in computer-compatible form.

The color monitor is a 12-inch Conrac Model 5521 RGB monitor from the Conrac Corporation in Covina, California. Because the microcomputer and random access memory have access times longer than that required to supply the color monitor for operation at standard scan rates, the picture must be transferred from the RAM to a video raster and refresh generator. This device is from the Grennell Corporation of Santa Clara, California and is called Graphic Television Imaging GMR-26 System. Advertised as a system controller by Grinell, it is used as a solid state memory which is accessible in parallel over 8 words, thereby appearing to have an access time 8 times shorter than the MOS chips of which it is constructed. The memory dimensions of this video refresh generator are 256 by 256 picture elements of 12 bits each. However, since the 12 bits must encompass a three-color picture, only 4 bits are available for each of the three constituent colors. Six bits of the 8 bit words generated by the A/D converter in the camera head are transferred to the processor. Since the RAM has a 12 bit word, two 6 bit video pixels are packaged into

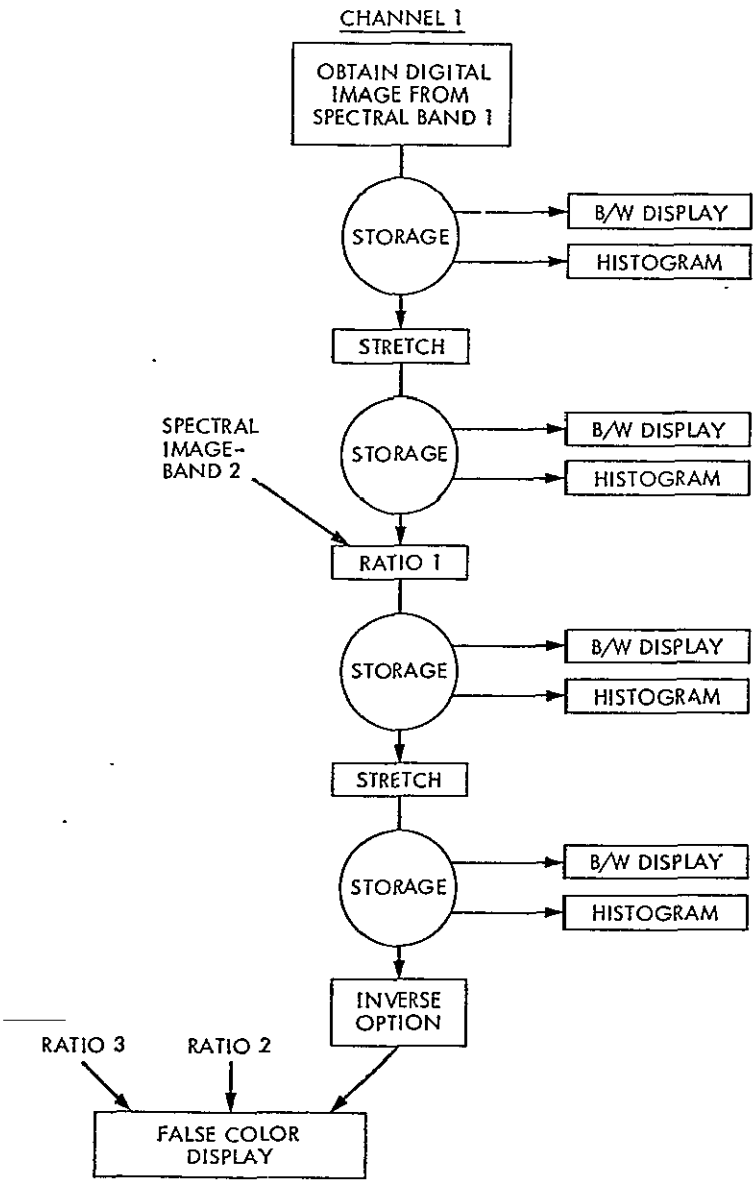

Figure 30. Analytical Protocol for Burn Diagnosis

The digital image received from the camera is immediately sent to a preselected storage area in the random access memory. Upon operator command from the keyboard, the brightness histogram and monochromatic image of a selected channel are displayed, the histogram on the keyboard monitor and the monochromatic image on the color monitor. The operator then chooses the parameters necessary to allow a contrast enhancement or stretch so that the dynamic range of the target area of the image matches that of the display device. Having selected these parameters, a software routine performs the contrast enhancement and places the stretched images back into storage in the random access memory and in a different storage area so that the initial data is preserved. The contrast enhanced image with its associated histogram is produced to confirm that the stretch accomplished its intended objective. If not,

the original data can be reconditioned with a new set of parameters. If the stretch is acceptable, the inter-ratio of the three channels is formed, i.e. (channel 1/channel 2), (channel 1/channel 3), and (channel 2/channel 3). The first ratio is placed into the memory in place of the original data of channel 1, the second into channel 2, and the third into channel 3. The monochromatic image of each channel can be displayed with its brightness histogram. It may be necessary to provide a contrast enhancement of this ratioed image using the approach described earlier. This is accomplished with a keyboard command. This step may be useful to provide improved color resolution of the final pseudocolor image. If not, the results of the analysis is presented by assigning the image in channel 1 to the red input of the RGB monitor, channel 2 to the green input, and channel 3 to the blue input. At this point it may be desirable to invert one of the monochromatic images, i.e., to assign black to white, and white to black. The resulting pseudocolor image as displayed on the color monitor is then used as the diagnostic image, the color presented being indicative of the depth of burn as discussed in Section III.

4. Random Access Memory Map

A map of the random access memory is presented in Figure 31. This figure is so titled for traditional reasons but in actuality it is a map of the addressing capability of the microprocessor. Although the memory has 112,000 locations, the 16 bit addressing capability of the microprocessor limits the system to 65,536 of those locations. This

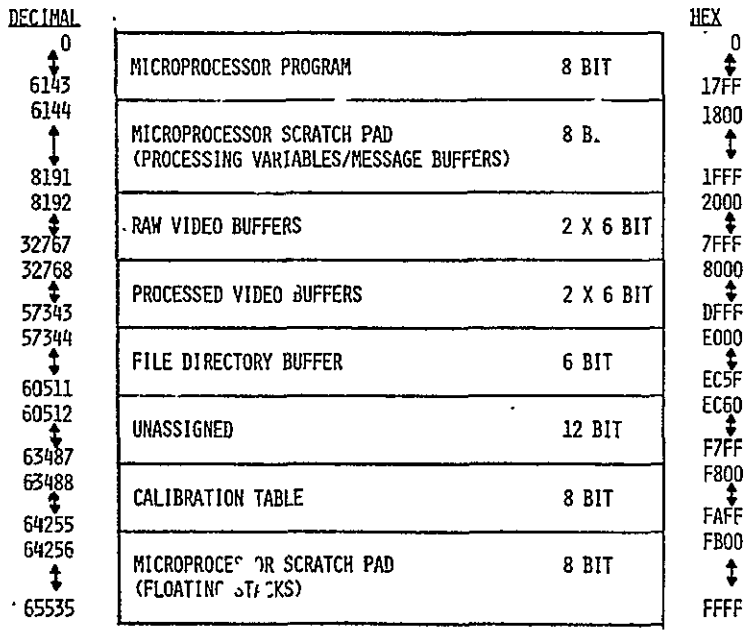

Figure 31. Memory Map

has presented a major problem in the design and implementation of the system. An approach to solving this problem was to page the memory with the processor's Q flip-flop output. This provides the 17th address bit to the memory. All video processing is then performed in pairs, and 16k video bytes are stored in 8k memory words. Processing is done on the lower 8k of a frame by setting Q low, then on the higher 8k by setting Q high. These correspond to the lower and upper six bits of a memory word. Because these processes share the same memory, it was necessary to incorporate special address decoding to allow for 8 bit read/write operations. Processor instructions and scratch pad operation and areas are not affected by Q. Memory expansion can be achieved by dedicating a separate memory to the processor and treating video memories as peripheral devices.

The bulk of the memory is reserved for original and processed video data. One monochrome frame requires 16,384 6 bit words using 8,192 addresses of the memory. With three frames of data and two storage locations for each frame, one for the data being processed and one for the processed data, there is the need for 49,152 addresses in memory. These addresses form the six frames of video buffer available. These are shown as the third and fourth entry in the memory map and account for a total of 49,152 addresses out of a total of 104,256. The remainder of the addressing capability of the system is designated as described in Figure 7.

5. Multispectral Camera Command Dictionary

The Medical Camera System is designed to take and process three-color images. The three spectral channels are labeled 1, 2, and 3.

The processor memory contains two data buffers, R and S, each large enough to store a complex three-color image. The various processing algorithms move the data back and forth between buffers, as explained below. The six monochrome images stored in the system are identified by the buffer and channel number, e.g., R2.

The program consists of a SUPERVISOR and several subroutines. When the system is under control of the SUPERVISOR, it will accept instructions from the keyboard to carry out any selected subroutine. With one exception (see below), the system will not accept a new instruction before the previous instruction has been completed. The system automatically returns to SUPERVISOR control whenever

(1) Power is switched on.

(2) The previously commanded subroutine is completed.

(3) The CONTROL and BREAK keys are depressed simultaneously. Control break is the one instruction accepted by the processor in the middle of a subroutine.

A beep tone is used to indicate that the previous instruction has been carried out, and that control has reverted to the SUPERVISOR.

The instruction dictionary for the available subroutines is given below:

Dictionary

T = Take. Prepares the system to take a new three-color picture. The picture is actually taken by depressing the push button on the camera head. The new picture is stored in both the R and S buffers.

M = Monochrome Display. Must be followed by buffer and channel identifiers. Thus, the instruction MS2 will result in a black and white display of the Channel 2 data in the S buffer.

H = Histogram. Must be followed by buffer and channel identifiers. Displays a brightness histogram on the terminal CRT and the corresponding monochrome image on the monitor.

C = Color Display. Displays the contents of the S buffer as a three-color picture on the monitor.

S = Stretch. Must be followed by buffer and channel identifiers. Results in a contrast change for the picture. Terminal will prompt operator for stretch parameters. When X = appears, enter the DN that will go to black. Then enter a comma, and Y = will appear. Enter the DN that will go to white, and close instruction with a period. Example X = 5, Y = 42. Stretched data is placed in the S buffer with the same channel number.

I = Inverse. Must be followed by a channel number. Operates only on S buffer. Converts picture to its inverse, i.e., white and black are interchanged. Places results back in S buffer with same channel number.

RA = Ratio. Operates on the three component pictures in the S buffer and writes results in R buffer. The three ratios computed by this subroutine are as follows:

$$\frac{c \times S1}{S2} \rightarrow R1$$

$$\frac{c \times S1}{S3} \rightarrow R2$$

$$\frac{c \times S2}{X3} \rightarrow R3$$

C is a multiplicative constant selectable by the operator which serves to preserve significant figures in the computation of the ratio. For example if C = 10 were selected then we would preserve one additional digit in the computation of the ratio. C, however, cannot be arbitrarily large or some of the quantities in R1, R2 or R3 would exceed the dynamic range of the 6 bit system.

RED = Read Directory. The first file on the tape contains a list of pictures that have been recorded. This command reads the directory and lists FILE NUMBER, DATE, and PATIENT NAME. The CRT has space for 24 list elements. If more than 24 video files exist, they can be listed by successive depressions of the NEW LINE key. The maximum number of files is 99.

REF = Read File. The prompt is NUMBER, and must be satisfied by keying in a two-digit file number. The tape recorder will then do a high-speed search to the desired file and read it into the R buffer. Patient Name, Date, Annotation Data, Stretch, and Inverse parameters are displayed on the CRT.

W = Write Tape. The operator is asked if the tape is new. A YES answer will result in another question: ARE YOU SURE? A second YES will save R buffer video and processing parameters in video file number one and start a new file directory. A NO to the first question will read the directory, add a new file an N + 1, write the updated directory, search to the next unused portion of the tape, and write the video file. NO to the second question results in a return to the SUPERVISOR.

A = Annotate. The operator may type in up to 4.8 CRT lines of data about the patient. If typing errors occur, they may be corrected by the use of the back arrow symbol (←). Each depression of this key will back space the buffer one place. Example: CAST ← ← ← OST = COST. To exit the annotation routine, the $ symbol is entered. An automatic exit occurs if the buffer is exhausted (4.8 lines). This information will be written on the tape with the next video write request.

D = Date. It must be entered as MM/DD/YY. Return to SUPERVISOR is automatic.

P = Patient's Name. Type in the name and terminate by depressing NEW LINE. The name buffer can accept up to 34 letters.

E = Edit. This is a program edit routine and is not for general use. Should it be entered inadvertently, depress control and break to return to the SUPERVISOR. This instruction is not available if the program has been loaded from the PROM.

X = Exchange. This program exchanges all images in the R and S buffers. For example R1 goes to S1 and S1 to R1, etc.

FILX = Filter (low pass). This subroutine causes a 3 x 3 low pass filter algorithm to be applied to the X image of the S-buffer. The new filtered images are placed into the R-buffer. If X = 1 (FIL1), the filter is applied only to channel 1; similarly, if X = 2, or 3, the filter applies to only that channel. If X = A, the filter applies to all channels. If $X_{2,2}$ is the center element of the 3 X 3 array, the algorithm used by the filter is

$$X_{2,2} = \frac{1}{9}\sum_{i=1}^{3}\sum_{j=1}^{3}.11\ X_{i,j}$$

This algorithm is applied to each pixel of the image using the original data of the image in the S buffer.

FIHX = Filter (high pass). This subroutine performs a high pass filter operation on the images of the S buffer in a 3 X 3 matrix and places the filtered images into the R-buffer. It is the complement to the low pass filter algorithm. X may be 1, 2, or 3 for individual channels or A for all channels.

FO = Focus. This subroutine allows a quick view of the image in the R1 buffer. It is entered on the keyboard and actuated by the push button on the camera. The purpose of this is to allow the camera to be aimed and focused without going through the more time consuming "take" command. Exit from focus by control break.

N = Negative Sum Inverse. This subroutine takes the absolute value of the difference between the images in the S-buffer and the R-buffer. It then performs the inverse (see subroutine I) of the result. The data resides in the R-buffer.

G = Go Sequence. This subroutine causes an automatic sequence of events as follows:

1. Histogram of R1 is shown on keyboard monitor; R1 is shown on TV monitor.

2. Automatic stretch of R1 is made for $\pm 2\sigma$ about mean; the stretched image is sent to S1.

3. Histogram of S1 is shown on keyboard monitor and image S1 is shown on TV monitor.

4. Steps 1, 2, 3 are repeated for R2 → S2.

5. Steps 1, 2, 3 are repeated for R3 → S3.

6. The ratio S1/S2 is taken, multiplied by 32 and stored in R1.

7. The ratio S1/S3 is taken, multiplied by 32 and stored in R2.

8. The ratio S2/S3 is taken, multiplied by 32 and stored in R3.

9. Steps 1, 2, 3, 4, 5 are repeated with the new images in R1, R2, R3.

10. The color image of the data in S1, S2, and S3 is presented on the TV monitor.

SECTION VII

OTHER APPLICATIONS OF MULTISPECTRAL ANALYSIS

During the course of the burn program the opportunity arose for consideration of other applications of multispectral analysis in medical diagnosis. These studies used either the photographic or the television systems and were conducted to determine the feasibility of using the multispectral analysis technique for the characterization of a particular pathological or physiological condition. A review of these applications is presented in this section.

A. PERIPHERAL VASCULAR DYNAMICS

The ability of the heart to provide blood to the extremities and of the extremities to accept this blood is easily shown by a safe, although objective test. This test is accomplished by directing a volunteer to be seated in a chair and allowing both arms to rest comfortably on the knees. The volunteer is then instructed to raise one hand, e.g., the right, high above the head for a period of two minutes. The blood flow to the raised arm is reduced and the hand appears less red in color. The raised arm is then lowered and placed adjacent to the undisturbed arm and the difference in the color tone is noted visibly. Within 60 seconds, the two hands appear nearly the same. Variations of this experiment would also allow the raised arm to indicate a hyperaemic effect. This would be caused by elevating the arm for extended periods of time.

Figure 32 shows the results of a study such as this taken by a photographic measurement of the spectral reflectance of both hands. The data are presented as the ratio of the reflectance of the right hand (after being raised) to that of the left hand (undisturbed), ρ_R/ρ_L, versus time after lowering the right hand. The data presented are for three serially conducted tests on a healthy, 20 year old male with no known vascular disease. Because the tests were serially conducted, they cannot be directly compared with each other. Three wavelength regions included were in the red, the green, and the very near infrared.

The green spectrum was the first test conducted. It shows a simple damping effect of the vascular system with the reflectance ratio returning to unity in about 90 seconds after the right arm was lowered. The second test was started immediately by raising the right arm for another period of 2 minutes. After lowering the arm, the reflectance data in the red spectra were taken. The response of the vascular system has then become more complex but again indicates the trend to return to normal. The right arm was immediately raised again, this time for a period of 3 minutes. Upon lowering the arm the infrared data were taken. This data again shows a complex response without a return to normal in 70 seconds. This is indicative of the hyperaemic response which probably begins at about 35 seconds after lowering the arm and continues beyond the length of the test.

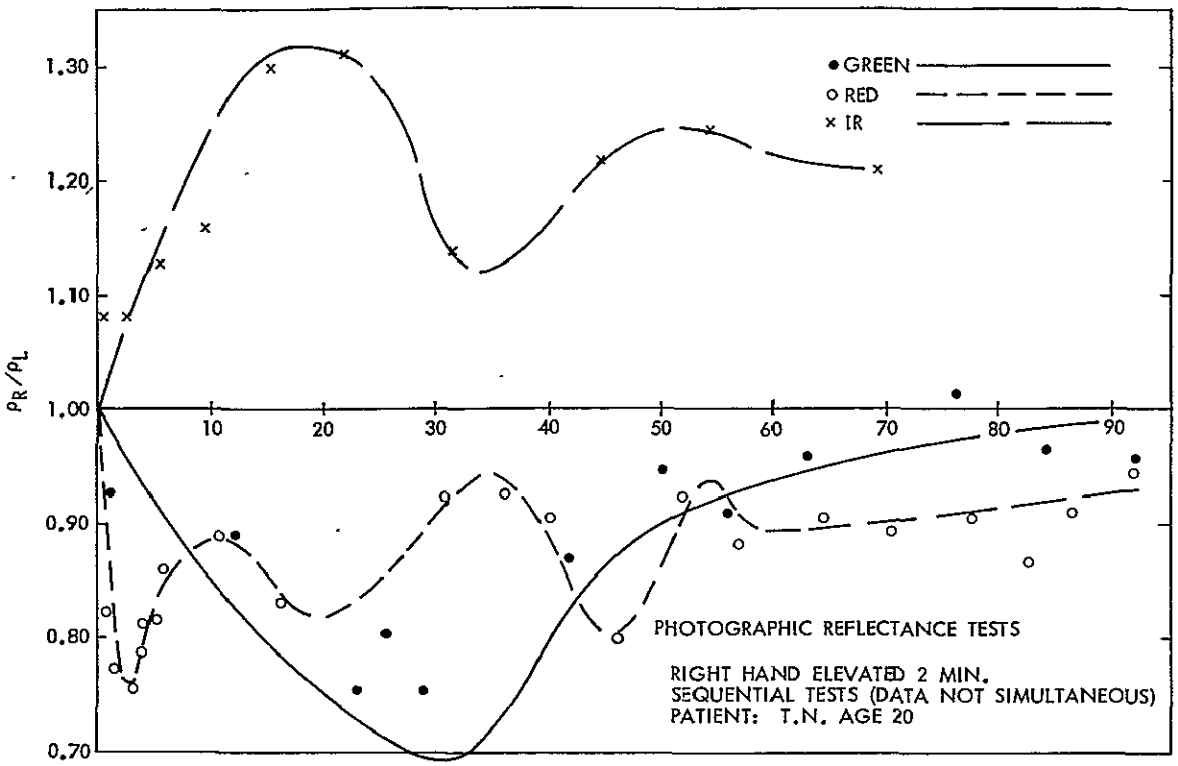

Figure 32. Dynamic Peripheral Vascular Study

Although of a preliminary nature, these tests show the ability to measure the dynamic response of the peripheral vascular system using spectral reflectance methods, and in particular, imaging methods. It is not clear which wavelengths are most important. That information could only result from a larger series of tests. There is, however, a strong possibility of using these types of tests for monitoring the presence of arterial or heart disease.

B. DIABETES

The severity of a diabetic condition in humans is often reflected by the state of the blood circulation in the skin. Disease of the peripheral vascular system causes reduced or inadequate perfusion of the skin, which often results in tissue breakdown.

Figure 33 shows spectral absorptance data taken from the right lateral heel of a patient with diabetes. Two conditions are shown. The first, indicated as a "pre-heat" condition, was taken while the patient was resting, seated in a wheelchair with the right foot elevated and horizontal. The temperature in the left post-tibial region at this time was 89.7°F. The legs were then heated by a lamp and the left post-tibial temperature rose to 94.1°F. This heating was accomplished to stimulate vasodilation and thereby increase the tissue perfusion. The second set of data, called the "post-heat" condition,

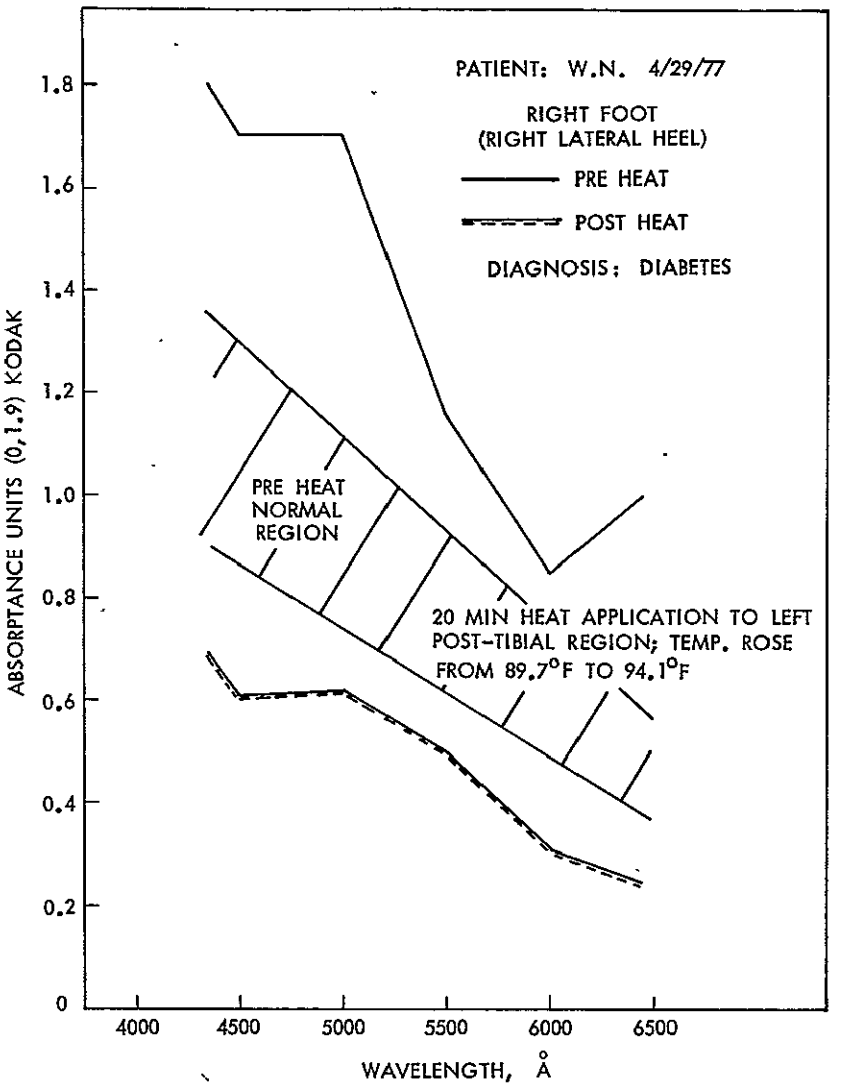

Figure 33. Spectral Reflectance of Patient with Diabetes

was then taken. Data at this time shows a considerable reduction in the skin absorption, indicating a large change in the skin perfusion. This is probably due to an increase in perfusion but this is not certain without further testing. In any case, the large change in absorptance shown in this experiment is quite different from that measured in normals in which case the pre-heat condition has much lower values as indicated in the figure.

C. MAJOR ARTERIAL OCCLUSIONS

A multispectral photographic analysis was conducted on a patient with a 90% occlusion of the left iliac artery. With the patient resting in bed, no visible differences in colorimetry could be seen between the right and left legs. Doppler pressures and temperatures were measured

at fixed locations on the right and left thighs, calves, and ankles. These were done in a resting condition (pre-heating) and after heating the legs with a lamp (post-heating) to induce vasodilation. The pressures and temperatures are shown in Figure 34. Note the variation in the pressure waveform and the reduction in systolic pressure which consistently appears in the left leg. Even under resting conditions, the temperatures of the left leg were lower, indirectly indicating a reduction in skin perfusion.

After heating, the pressures of the right leg were reduced in the thigh, leg, and ankle by 12, 10, and 4 mm Hg, respectively. In the left leg, however, the pressure changed erratically. The thigh pressure dropped 30 mm Hg, the calf pressure rose 6 mm Hg and the ankle pressure dropped 6 mm Hg. No definitive reason was given for this result; however, it was speculated that the effect was due to the development of a collateral circulation which would not respond in a symmetrical way with the right leg.

The multispectral absorptances of both legs, before and after heating, are shown in Figures 35 and 36. Figure 35 shows the preheating condition. Note the large difference in the absorptance values between the legs due to the occlusion in the left iliac. After heating, there was a general trend for the absorptance values to diminish, with the left leg still being lower than the right with the exception of the right thigh. It is speculated that this condition may be due to the development of colateral vessels in the pelvic region having an effect on the left side.

The data presented in Figures 35 and 36 in general show a consistent difference in the states of the peripheral circulation between a basically normal and a diseased leg. This was accomplished by imaging methods in a simplified and preliminary manner. It is expected that pseudocolor imagery, similar to that used by the burn diagnostic work, could be useful in detecting deep vascular disease.

These discussions summarize several areas of potential use for multispectral imaging in medicine. The applications are based on the ability of multispectral analysis to monitor, with the use of images, the variation in blood flow through the skin. This method of analysis can be explained by reference to the graph of Figure 37. The vertical axis is the perfusion density or the amount of oxygenated hemoglobin in the skin. This is measured by noting the "redness" of the skin and would increase from unperfused tissue to a state of hyperaemia. Decreasing the oxygen concentration of the cutaneous blood increases the "blueness" of the skin. This is shown as the horizontal axis. Finally, insofar as the application to burns is concerned, the third axis to be considered is that which indicates changes in the state of cutaneous blood due to thermal denaturation of the blood. The implication is that there is some process by which thermal injury to the skin increases the actual infrared absorptance, or the effective absorptance, measured through the skin. By using these axes, one defines spatial

PRE-THERMAL

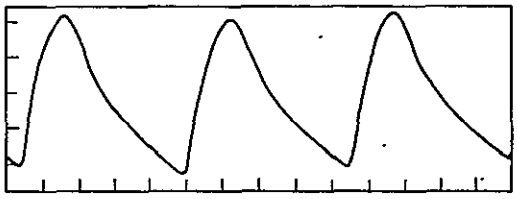

RIGHT THIGH: Psys = 152 mm Hg
T = 90.5°F

A

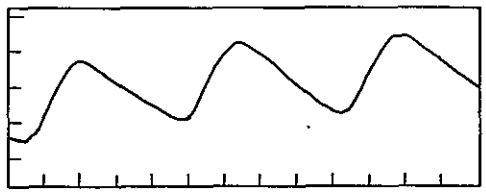

LEFT THIGH: Psys = 122 mm Hg
T = 89.8°F

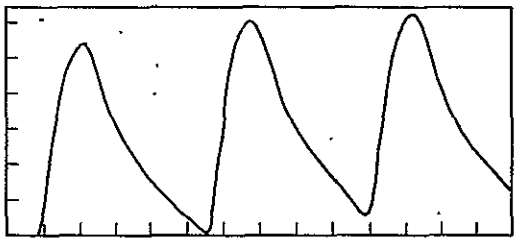

RIGHT CALF: Psys = 146 mm Hg
T = 89.9°F

B

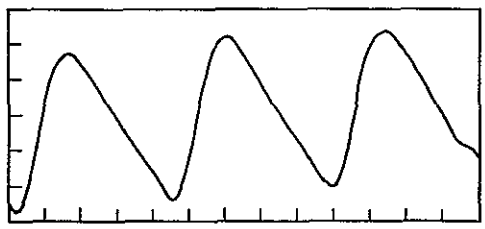

LEFT CALF: Psys = 96 mm Hg
T = 88.8°F

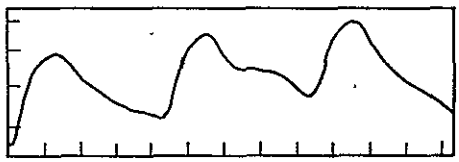

RIGHT ANKLE: Psys = 138 mm Hg
T = 86.8°F

C

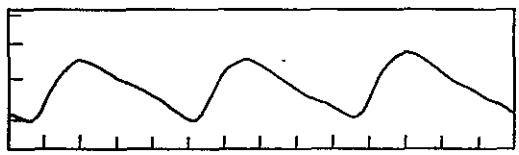

LEFT ANKLE: Psys = 112 mm Hg
T = 86.1°F

POST THERMAL

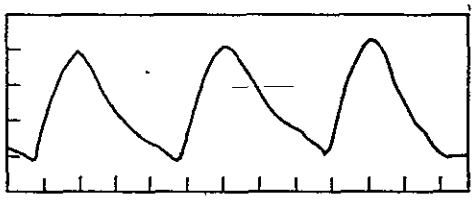

RIGHT THIGH: Psys = 140 mm Hg
T = 94.6°F

D

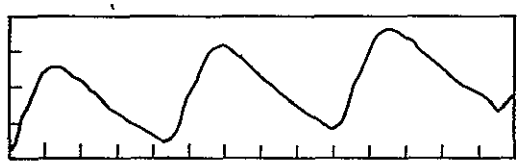

LEFT THIGH: Psys = 92 mm Hg
T = 94.7°F

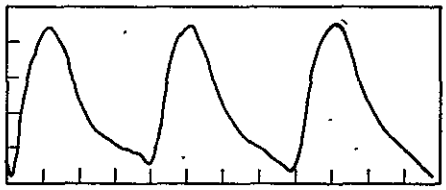

RIGHT CALF: Psys = 136 mm Hg
T = 96.0°F

E

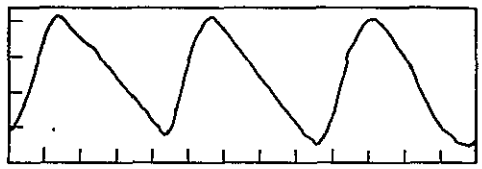

LEFT CALF: Psys = 102 mm Hg
T = 96.1°F

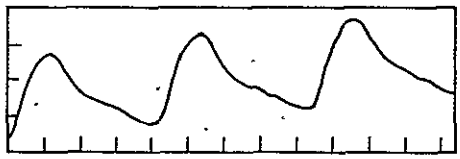

RIGHT ANKLE: Psys = 134 mm Hg
T = 94.6°F

F

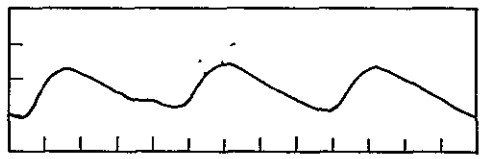

LEFT ANKLE: Psys = 106 mm Hg
T = 94.2°F

Figure 34. Clinical Temperatures and Pressures

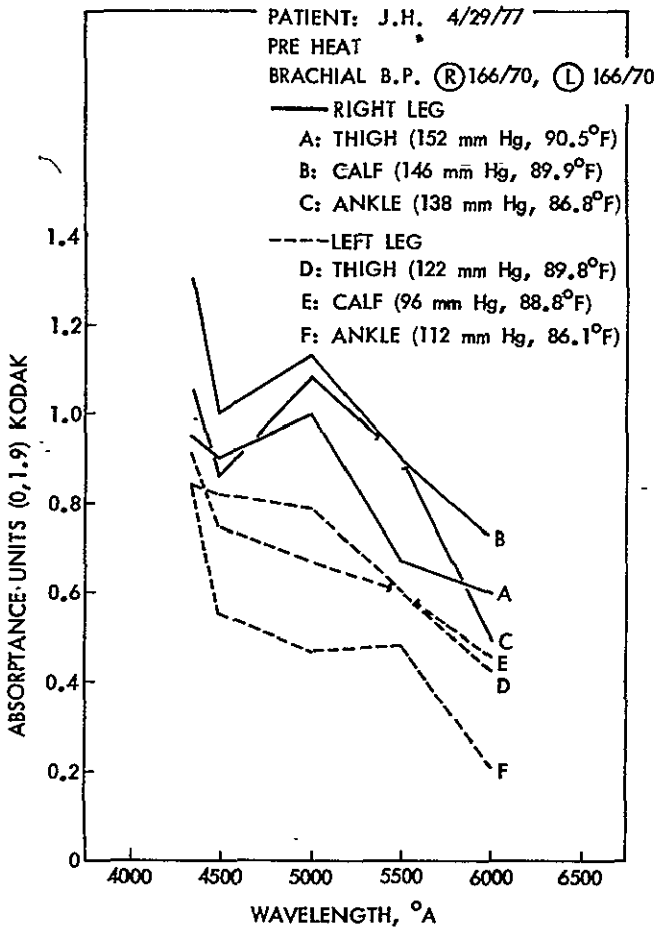

Figure 35. Pre-Heating Spectral Absorptance

positions of normal or abnormal characteristics. These determinations are automatically accomplished by the computational procedures of multispectral analysis and the results are typically presented by pseudocolor variations of the target being studied.

Much work remains to be accomplished in the application of multispectral imaging to the diagnosis of burns as well as to the other areas discussed in this report. The potential for accomplishing noninvasive diagnosis of various dermatological and vascular diseases is shown. Feasibility studies, followed by clinical trials, must now be considered for particular applications.

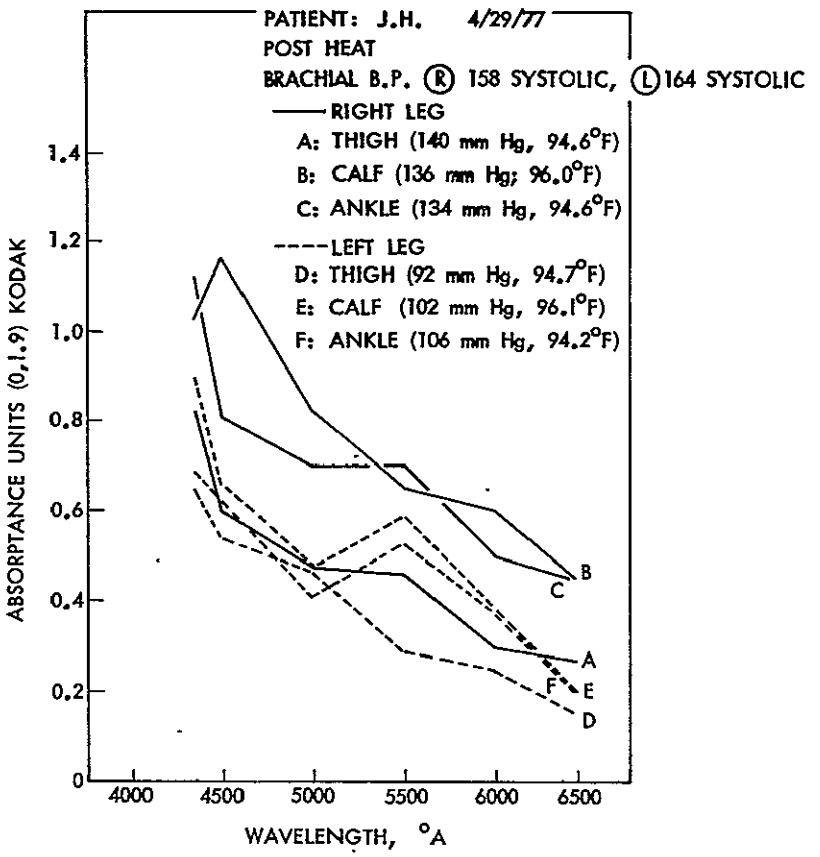

Figure 36. Post-Heating Spectral Absorptance

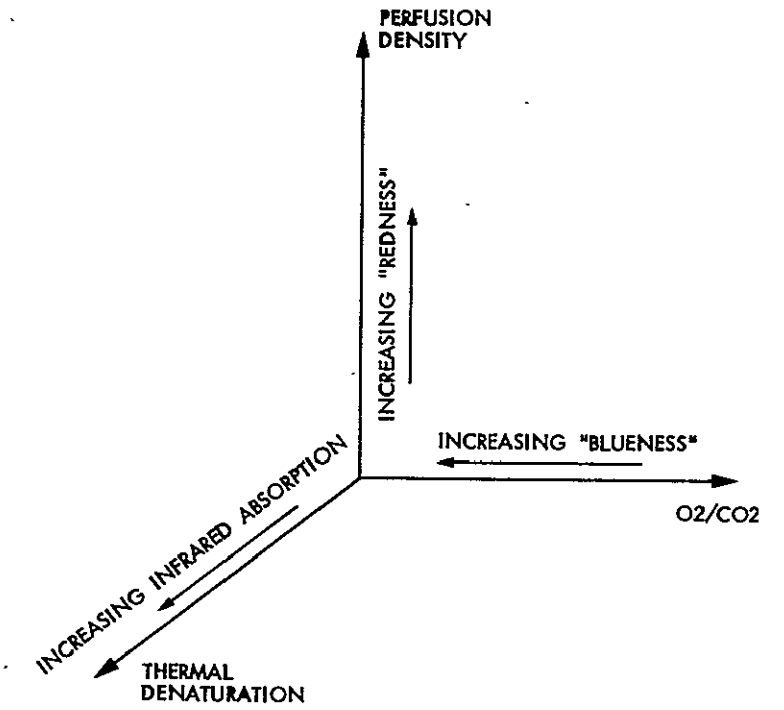

Figure 37. Cutaneous Blood Flow Parameters

REFERENCES

Anselmo, V. J., and Zawacki, B. E., 1973, "Infrared Photography as a Diagnostic Tool for the Burn Wound," Proceedings of the Society of Photo-Optical Instrumentation Engineers, Quantitative Imagery in the Biomedical Sciences - II, Vol. 80, pg. 181.

Anselmo, V. J., and Zawacki, B. E., May 1977, "Effect of Evaporative Surface Cooling on the Thermographic Assessment of Burn Depth," Radiology, Vol. 123, No. 2, pp. 331-332.

Anselmo, V. J., and Zawacki, B. E., June 1977, "Multispectral Photographic Analyses: A New Quantitative Tool to Assist in the Early Diagnosis of Thermal Burn Depth," Annals of Biomedical Engineering, Vol. 5, No. 2, pp. 179-193.

Goetz, A. F. H., et al., 1975, Applications of ERTS Images and Image Processing to Regional Geologic Problems and Geologic Mapping in Northern Arizona, TR-32-1597, Jet Propulsion Laboratory, Pasadena, CA.

Hinshaw, J. R., 1961, "Why Burn Severity is Often Misjudged," Archives of Surgery, Vol. 83, pp. 81-85.

Jackson, D. MacG., 1953, "The Diagnosis of the Depth of Burning," British Journal of Surgery, Vol. 40, pp. 588-596.

Jackson, D. MacG., 1961, "A Uniform Classification of the Depth of Burns," in Research in Burns, P. Mather, T. L. Barclay, and F. Konickova (Eds.), Bern: Huber, pp. 713-714.

Jackson, D. MacG., 1969, "Second Thoughts on the Burn Wound," The Journal of Trauma, Vol. 9, pp. 829-862.

Jackson, D. MacG., and Stone, P. A., 1972, "Tangential Excision and Grafting of Burns," British Journal of Plastic and Reconstructive Surgery, Vol. 25, pp. 416-426.

Janzekovic, Z., 1970, "A New Concept in the Early Excision and Immediate Grafting of Burns," The Journal of Trauma, Vol. 10, pp. 1103-1108.

Monafo, W. W., Aubenbacher, C. E., and Pappalardo, C., 1972, "Early Tangential Excision of the Eschars of Major Burns," Archives of Surgery, Vol. 104, pp. 503-514.

NIH Record, Feb. 13, 1973, National Institutes of Health, pg. 4.

Sevitt, S., 1957, Burns, Pathology and Therapeutic Applications, London, Butterworth, pg. 19.

Walker, H. L., and Mason, A. D., Jr., 1968, "A Standard Animal Burn," The Journal of Trauma, Vol. 8, pg. 1049.

Zawacki, B. E., and Jones, R. J., 1967, "Standard Depth Burns in the Rat: The Importance of the Hair Growth Cycle," British Journal of Plastic and Reconstructive Surgery, Vol. 20, pp. 347-354.

Zawacki, B. E., 1974, "Reversal of Capillary Stasis and Prevention of Necrosis in Burns," Annals of Surgery, Vol. 180, pp. 98-102.